

Physics, Instrumentation, and Radiation Protection

P. ZANZONICO, S. HELLER

1.1

Introduction

The underlying principles of nuclear medicine imaging involve the use of unsealed sources of radioactivity which are administered in the form of radiopharmaceuticals; the ionizing radiations which accompany the decay of the administered radioactivity can be detected and measured with specially designed instruments (e.g., survey meters, gamma cameras). In order to appreciate the scientific and technical basis of nuclear medicine imaging, this chapter reviews atomic and nuclear structure, radioactivity and radioactive decay, and interactions of radiation with matter. This is followed by a discussion of techniques for detection and measurement of radiation, design and operating principles of detection and imaging instruments, instrument quality control, and radiation protection.

1.2

Basic Physics

1.2.1

Atomic and Nuclear Structure

Matter is, of course, composed of atoms, which represent the smallest indivisible sub-unit of an element which retains the characteristic physical and chemical properties of that element. Atoms are composed of a nucleus surrounded by orbital electrons, with the atomic structure maintained by electrostatic forces of attraction between the positively charged nucleus and the negatively charged electrons. Nuclei are composed of positively charged protons and electrically neutral neutrons, which are collectively referred to as nucleons. Orbital electrons are negatively charged; in an electrically neutral, or uncharged, atom, the number of negative orbital electrons equals the number of positive nuclear protons, the charge on these respective particles being equal in magnitude. The properties of these fundamental building blocks of matter – electrons, protons, and neutrons – are summarized in Table 1.1. In addition, positively charged electrons (referred to as “positrons”) do not normally exist in nature but can be

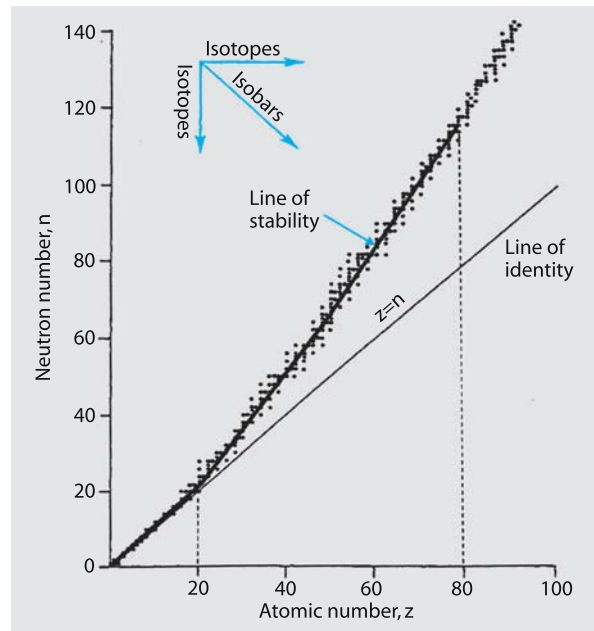


Fig. 1.1. The chart of the nuclides, a scattergram of neutron number, N , versus atomic number, Z , for all nuclides. Note that isotopes, isobars, and isotones lie along vertical, diagonal, and horizontal lines, respectively. Note further that structurally stable and therefore non-radioactive nuclei lie along the so-called “line of stability,” which runs through the center of this scattergram. The line of stability is bi-phasic, corresponding to the line of identity, $N = Z$, for small nuclei ($Z \leq \sim 20$) and to a steeper line, $N = 1.5Z$, for larger nuclei ($\sim 20 \leq Z \leq \sim 80$), and ends at $Z \approx 80$.

generated during certain modes of radioactive decay and only exist for very short periods of time (described below).

Nuclei are structurally characterized by three parameters: atomic number, Z – the number of protons; the neutron number, N – the number of neutrons; and the mass number, $A = Z + N$, the number of nucleons (i.e., neutrons and protons). The atomic number, Z , thus indicates the positive charge of the nucleus and indicates the chemical identity of the element. For example, an atomic number of “6” defines the atom as car-

Table 1.1. Properties of the fundamental particles of matter

Particle	Symbol ^a	Mass		Rest mass energy (E_0) ^b		Charge	
		Universal mass units (u) ^c	Grams (g)	keV ^d	MeV ^d	Elementary charge	Coulombs (C)
Electron	e						
Negatron	e ⁻	5.486×10 ⁻⁴	9.110×10 ⁻²⁸	511	0.511	-1	-1.602×10 ⁻¹⁹
Positron	e ⁺	5.486×10 ⁻⁴	9.110×10 ⁻²⁸	511	0.511	+1	+1.602×10 ⁻¹⁹
Proton	p/p ⁺	1.007	1.673×10 ⁻²⁴	938,000	938	+1	+1.602×10 ⁻¹⁹
Neutron	n/n ⁰	1.009	1.675×10 ⁻²⁴	939,000	939	0	0

^a In representing particles, the charge is often not explicitly indicated. In the case of electrons, the symbol e (without the charge indicated) is generally interpreted as identifying a negatron

^b From Einstein's Special Theory of Relativity, the rest mass energy E_0 of a particle of mass m is given by the equation, $E_0 = mc^2$, where c is the speed of light in vacuum, 3×10^8 m/s

^c In atomic and nuclear physics, energies are commonly expressed as universal mass units (u), 1/12 of the mass of a carbon-12 atom, 1.66054×10^{-27} kg

^d In atomic and nuclear physics, energies are commonly expressed as multiples of an electron-volt (eV), the kinetic energy of an electron after passing through a potential difference of 1 volt (V). An MeV, or mega-electron-volt, equals 1 million eV and a keV, or kilo-electron-volt, equals 1 thousand eV

	Energy, E			Frequency, ν		Wavelength, λ	
	eV	keV	MeV	Hz ^a	MHz ^a	m	nm
Radio, TV	10 ⁻⁸	10 ⁻¹¹	10 ⁻¹⁴	10 ⁶	1	10 ²	10 ¹¹
Microwave	10 ⁻⁴	10 ⁻⁷	10 ⁻¹⁰	10 ¹⁰	10 ⁴	10 ⁻²	10 ⁷
Infrared	0.1	10 ⁻⁴	10 ⁻⁷	10 ¹³	10 ⁷	10 ⁻⁵	10 ⁴
Visible	1	10 ⁻³	10 ⁻⁶	10 ¹⁴	10 ⁸	10 ⁻⁶	10 ³
Ultraviolet	10	10 ⁻²	10 ⁻⁵	10 ¹⁵	10 ⁹	10 ⁻⁷	10 ²
X- and γ -rays	10 ³	1	10 ⁻²	10 ¹⁸	10 ¹²	10 ⁻¹¹	10 ⁻²

Table 1.2. The electromagnetic (EM) spectrum

^a Frequencies are typically expressed in units of hertz (Hz), equal to 1 cycle/s (or 1/s). The unit of MHz, or megahertz, equals 1 million Hz and is commonly used to express frequencies of EM radiations

bon. In shorthand, carbon can be represented by just using the chemical symbol and the atomic number, or ¹²C. Based on these structural parameters, different nuclear “families” have been identified: “isotopes” (e.g. ¹⁰B⁵ and ¹¹B⁵) are nuclei having the same atomic number, Z , and thus are nuclei of the same element; “isobars” (e.g. ¹¹C⁵ and ¹¹B⁵) have the same mass number, A ; and “isotones” (e.g. ¹¹C⁶ and ¹⁰B⁵) have the same neutron number, N . A useful graphical representation of the atomic nuclei is shown in Fig. 1.1, plotting the neutron number, N , versus the atomic number, Z . For relatively small nuclei ($Z < 20$), the nuclei are clustered around the line of identity (i.e., the line $N = Z$); for larger nuclei, they cluster about a steeper line (i.e., the line $N = 1.5Z$).

In the parlance of modern physics, atoms and nuclei are “quantum” systems: the values specifying the positions and energies of particles comprising atoms and nuclei are discrete. Thus, orbital electrons are found only in orbits, or shells at discrete distances from the nucleus, as shown diagrammatically in the Bohr (or “planetary”) model of the atom (Fig. 1.2). Nucleons (i.e., protons and neutrons) are likewise arranged in discrete energy levels, or shells within the nucleus. The electron's binding energy, which holds the electron in

its orbit, decreases, and its potential energy increases with increasing distance from the nucleus.

Atoms are of the order of 10^{-10} m in diameter and nuclei only one-thousandth of that, 10^{-13} m, in diameter. Nuclear volumes are therefore only ~1 billionth of atomic volumes. The atom and therefore matter in general is thus almost entirely empty space! Nucleon masses, on the other hand, are more than 1,000 times the mass of electrons (Table 1.1) and therefore virtually all (> 99%) of the “mass” of the atom and of matter generally is found in the nucleus.

In so-called “ground-state” atoms, orbital electrons occupy the shells (i.e., energy levels) closest to the nucleus, that is, the lowest-energy levels. Likewise in ground-state nuclei, nucleons occupy the lowest-energy shells. At this time vacancies may be created producing a non-ground state, or “excited,” atoms and nuclei. In such instances, electrons or nucleons will spontaneously move to fill these vacant lower-energy shells. In the process energy is released from the atom in the form of electromagnetic radiation (Table 1.2). This photon energy is equal to the difference between the initial and final potential energies of the electron or nucleon (Fig. 1.3a). In an atom, electron transitions from an outer shell to an inner shell result in the emission of

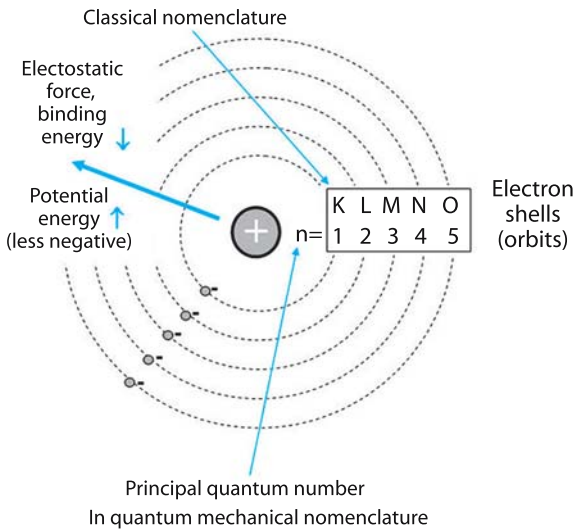


Fig. 1.2. In the Bohr (or planetary) model, the atom is depicted as a miniature solar system, with a positively charged nucleus at the center and negatively charged orbital electrons at discrete (or quantized) radial distances away. Each electron's radial distance from the nucleus, and therefore its shell (or orbit) and its potential energy, are indicated by its principal quantum number n [beginning with the value 1 for the innermost, or lowest (most-negative) potential energy, shell and ascending in numerical order for further, higher-potential energy shells]. An alternative designation of the respective electron shells begins with the letter K for the innermost shell, ascending in alphabetical order for the further shells. Although not shown, each shell is composed of more closely spaced sub-shells and ultimately orbitals (designated, in order of increasing potential energy, as s, p, d, and f). There may be up to two electrons – one with spin “up” and the other with spin “down” (corresponding to spin quantum numbers $+1/2$ and $-1/2$, respectively) – per orbital. A shell with principal quantum number n may contain up to n^2 orbitals and therefore up to $2n^2$ electrons

high-energy X-ray photons. The kinetic energy of the emitted X-ray is described in terms of electron volts, or eV; an eV is the increase in kinetic energy as an electron is accelerated through a potential of 1 V. Likewise, in a nucleus, nucleon transitions result in the emission of photons, or gamma (γ) rays. These photons have energies on the order of keV (10^3 eV) and MeV (10^6 eV). The energy of these photons is “characteristic” and defines the atom from which they originated. The defining difference between X- and γ -rays is related to where they originate – X-rays from the orbital electrons and γ -rays from within the nucleus.

Excited atoms and nuclei do not always result in the emission, respectively, of X- and γ -rays. In the case of excited atoms, the energy released as an orbital electron transitions from an outer to an inner shell may instead be transferred to another orbital electron within the same atom, ejecting the latter electron. The electron thus ejected is termed an “Auger electron” (Fig. 1.3b). The “fluorescent yield (ω_K)” is the probability that a shell-to-shell electron transition will yield characteristic X-rays rather than Auger electrons. This ratio increases with increasing atomic number and reaches a value of ~ 1 (i.e., all X-ray and no Auger-electron emission) by an atomic number of ~ 50 . In the case of unstable nuclei, the energy released as a nucleon transition from a higher- to a lower-energy shell likewise may instead be transferred to an orbital electron within the same atom, ejecting that electron from the atom. This process is called “internal conversion” and the ejected electron is termed a “conversion electron” (Fig. 1.3c).

Some nuclei may exist in different energy states (e.g., ground and excited states) and are referred to as “isomers”; the transition from an excited state to its ground state is termed an “isomeric transition.” Typically, excited nuclear states are very short-lived (of the order of 10^{-12} s or less). Certain excited nuclear states, however,

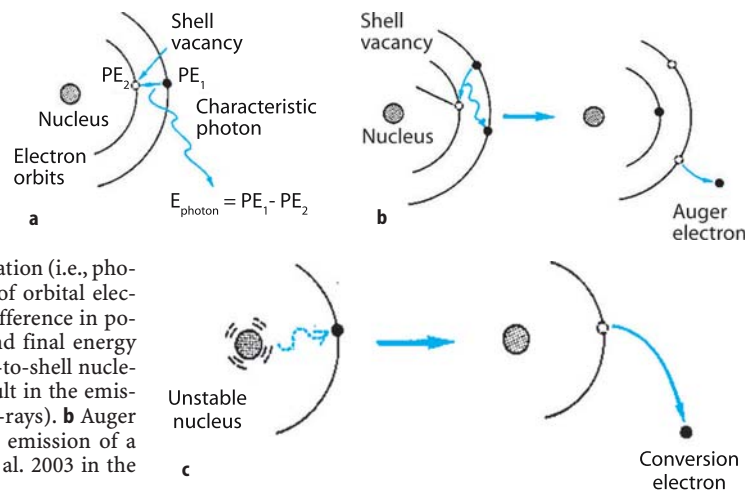


Fig. 1.3. **a** Emission of characteristic atomic radiation (i.e., photon) resulting from a shell-to-shell transition of orbital electrons. The photon energy, E_{photon} , equals the difference in potential energies of the electron in its initial and final energy levels, PE_1 and PE_2 . Analogous processes, shell-to-shell nucleon transitions, occur in atomic nuclei and result in the emission of characteristic nuclear radiations (i.e., γ -rays). **b** Auger electron emission. **c** Internal conversion, with emission of a conversion electron. (Adapted from Cherry et al. 2003 in the “Further Reading” list)

are unusually long-lived (with lifetimes of the order of seconds to hours) and are referred to as “metastable” (or “almost-stable”) states. Metastable nuclei are indicated by the letter “m” immediately following their mass number A ; thus, ^{99m}Tc is a metastable excited state of ^{99}Tc and ^{99m}Tc and ^{99}Tc are isomers of technetium-99.

1.2.2

Radioactivity

1.2.2.1

Nuclear Instability

Radioactivity is a property of atomic nuclei and may be defined as the spontaneous transformation of a structurally unstable nucleus to a structurally more stable nucleus, with the emission of energy in the form of ionizing radiation. Two features largely determine the structural stability of a nucleus, the size (i.e., atomic number, Z) and the neutron-to-proton (N -to- Z) ratio. All large nuclei (i.e., $Z \gtrsim 80$) are structurally unstable and therefore radioactive. For nuclei with an atomic number $Z \lesssim 80$, structural stability depends on the neutron-to-proton (N -to- Z) ratio. For small nuclei (i.e., $Z \lesssim 20$), stability is achieved for nuclei having an equal number of neutrons and protons, that is, an N -to- Z ratio of 1. For larger nuclei (i.e., $\sim 20 \leq Z \leq \sim 80$), stability is achieved for nuclei having three neutrons for every two protons or an N -to- Z ratio of 1.5.

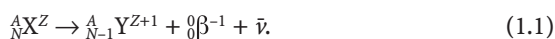
1.2.2.2

Modes of Radioactive Decay

The position of a nuclide on the chart of the nuclides determines its mode of radioactive decay. Nuclei of elements with ($Z \gtrsim 80$) lie *above* the line of stability and are unstable; they become more stable by generating and emitting an alpha (α) particle.

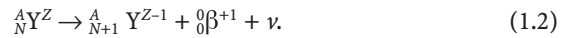
An α -particle, consisting of two neutrons and two protons, is structurally identical to a helium-4 nucleus, $^4_2\text{He}^2$ and α decay reduces nuclear mass by 4. α -particles are emitted from an unstable nucleus and are monoenergetic, having a kinetic energy that is specific to the nuclei (typically of the order of 5 MeV).

For small nuclei ($Z \lesssim 80$) lying to the *left* of the line of stability, their N -to- Z ratio is unstably high – that is, they have an excess of neutrons and become more stable by converting a neutron to a proton and a beta (β) particle, referred to as beta-minus (β^-) decay:

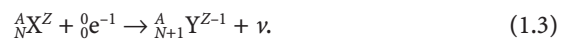


A β^- -particle is structurally identical to an electron, e^- , and β^- decay reduces the unstably high N -to- Z ratio to a more stable value, $(N-1)/(Z+1)$. The emission of a β^- -particle is always accompanied by the emission of a charge-less and mass-less particle known as an anti-neutrino, $\bar{\nu}$.

For small nuclei ($Z \lesssim 80$) lying on the opposite side – to the *right* – of the line of stability, their N -to- Z ratio is unstably low – that is, they have a deficiency of neutrons – and become more stable by converting a proton to a neutron and generating a beta-plus (β^+), or positron, particle, referred to as positron decay:



A β^+ -particle is also referred to as a positron and has the same mass as a negative electron. For these nuclei with an unstable, low N -to- Z ratio, there is, in addition, an alternative mode of decay called electron capture (EC), in which an intra-nuclear proton literally captures (i.e., combines with) an orbital electron and is thereby converted to a neutron:



Importantly, β^+ decay is only possible if the “transition energy, Q ”, the difference between the total mass plus nuclear binding energies between the two nuclei, exceeds an energy threshold of 1.022 MeV (= 1,022 keV). If the transition energy of the decay is less than 1.022 MeV, then *only* electron capture can occur. If, however, $Q > 1.022$ MeV, then both β^+ decay and electron capture can occur. Both β^+ decay and electron capture increase an unstably low N -to- Z ratio to a more stable value, $(N+1)/(Z-1)$, and are accompanied by the emission of a charge-less and mass-less neutrino, ν .

In beta (either β^- or β^+) decay and electron capture, the mass number, A , does not change. Therefore, beta decay and electron capture are known as “isobaric transitions.” In beta decay of a particular radionuclide, the electrons or positrons are emitted over a range of kinetic energies from zero to a radionuclide-specific maximum energy known as the “end-point energy, $(E_\beta)_{\text{max}}$.” A useful rule-of-thumb is that, for a particular radionuclide, the average β -ray energy, \bar{E}_β , is approximately one-third of the end-point energy.

Radioactive decay generally yields nuclei in excited (higher-energy) states, with dissipation of excess energy either by the emission of γ -rays or by internal conversion and emission of the resulting conversion electrons. The electron shell vacancies which result from internal conversion (or from electron capture), in turn, lead to electrons entering these inner shells and the emission of characteristic X-rays and Auger electrons. Thus, radioactive decay typically results in a complex cascade of events, beginning with the transformation of one nuclide to another and culminating in the emission of γ -rays, X-rays, and/or electrons.

1.2.2.3

Mathematics of Radioactive Decay

The physical quantity activity, “ A ”, specifies the amount of radioactivity and is the number of radioactive disin-

tegrations (or decays) which occur per unit time. Activity is commonly expressed in disintegrations per second (dps) or disintegrations per minute (dpm):

The conventional unit of activity is the curie (Ci), which represents 3.7×10^{10} dps. (This somewhat odd value is the number of dps in 1 g of radium.) Relative to the amounts of radioactivity used clinically, 1 Ci is a very large activity. Accordingly, sub-multiples of the curie are often used: 1 millicurie (mCi), 3.7×10^7 dps, is one-thousandth of 1 Ci and 1 microcurie (μ Ci), 3.7×10^4 dps, is one-millionth of 1 Ci. The newer, System Internationale (SI) unit of activity is the “becquerel (Bq),” which corresponds to 1 dps. In contrast to 1 Ci, 1 Bq is a very small activity, and so multiples of the becquerel are often used clinically: 1 kilobecquerel (kBq), 1×10^3 dps, is one thousand Bq and 1 megabecquerel (MBq), 1×10^6 dps, is one million Bq. Note that $1 \mu\text{Ci} = 37 \text{ kBq}$ and $1 \text{ mCi} = 37 \text{ MBq}$.

The mathematics of radioactive decay are well characterized and allow accurate and precise calculation of activities as a function of time. Radioactive nuclei decay (and become stable nuclides) in an exponential manner as a function of time, that is, for a given radionuclide the *fraction* of such nuclei decaying per unit time is constant and referred to as the physical decay constant λ , which is the fraction of radioactive nuclei decaying per unit time (e.g., 0.1 s^{-1} or 10% decaying per second). The practical form of the exponential law of radioactivity is written as:

$$N(t) = N(0)e^{-\lambda t} \quad (1.4)$$

$$\text{or} \quad A(t) = A(0)e^{-\lambda t} \quad (1.5)$$

where $N(t)$ = the number of radioactive nuclei remaining at the time t

$N(0)$ = the number of radioactive nuclei at time 0

$A(t)$ = the activity remaining at time t

$A(0)$ = the activity at time 0

The quantity $e^{-\lambda t}$ is the so-called “decay factor,” the fraction of activity remaining at time t . The appearance of the exponential law of radioactive decay (Eq. 1.4) on various types of graphs is presented in Fig. 1.4. Note, in particular, that such an exponential function appears as a straight line when plotted on a semi-log graph (Fig. 1.4c).

In addition to the physical decay constant, λ , there are other quantities which express the rate of decay of a given radionuclide: the half-life, $T_{1/2}$, which is the time interval for the number of disintegrations/s (decay rate) to drop by 50% and the mean life, τ , is the time interval for one-half of a given number of radioactive nuclei to decay. The mean life is used in dosimetry calculations of radiation doses from internally administered radionuclides. The decay constant, λ , half-life, $T_{1/2}$, and mean life, τ , are mathematically related as follows:

$$\lambda = 0.693/T_{1/2} \quad (1.6)$$

$$\text{or} \quad T_{1/2} = 0.693/\lambda \quad (1.7)$$

$$\tau = 1.44 T_{1/2} \quad (1.8)$$

Combining Eqs. 5 and 6 yields the more common form of the decay equation:

$$A(t) = A(0)e^{-0.693t/(T-1/2)} \quad (1.9)$$

Note that when $t = T_{1/2}$ this equation correctly predicts that $A(t) = 0.5 A(0)$.

Radionuclides often decay not to a stable (i.e., non-radioactive) nuclide but rather to another radionuclide. The resulting radionuclide, of course, will itself subsequently undergo radioactive decay. Such sequences of parent (p), daughter (d), grand-daughter (g), etc., radionuclides are known as radioactive “families” and are the basis of radionuclide generators. The most important radionuclide generator is $^{99}\text{Mo}/^{99\text{m}}\text{Tc}$,

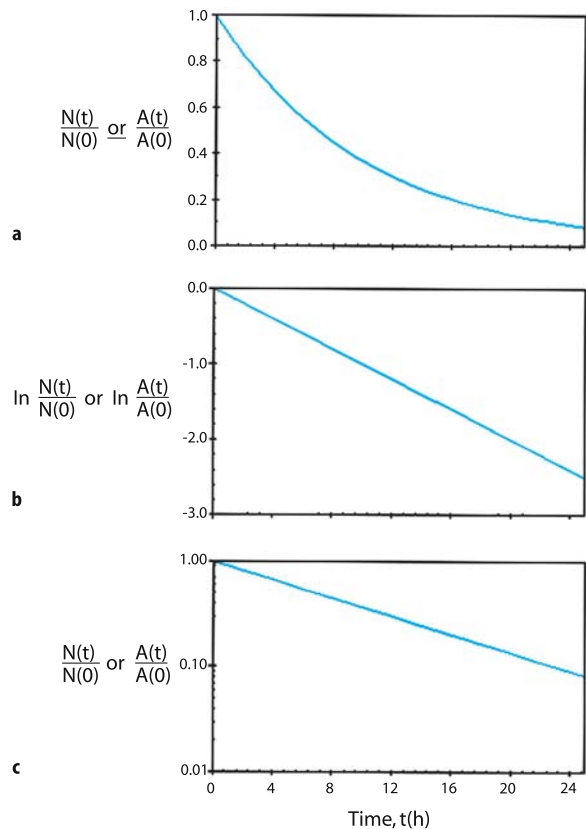


Fig. 1.4. Graphs of the exponential law of radioactive decay (Eqs. 1.4, 1.5): the fraction of the number of radioactive nuclei $[N(t)/N(0)]$ or of activity $[A(t)/A(0)]$ versus time (in hours), t , for a decay constant $\lambda = 0.1/\text{h}$. **a** Plotted on a linear-linear graph. **b** Plot of the log transform of the exponential law of radioactive decay, that is, the natural logarithm of $N(t)/N(0)$ or of $A(t)/A(0)$ plotted on a linear-linear graph. It appears as a straight line with a slope of λ and a y -intercept of 0. **c** When $N(t)/N(0)$ or $A(t)/A(0)$ is plotted on a semi-logarithmic (“semi-log”) graph, it again appears as a straight line

which is a parent-daughter radionuclide pair in a container that permits separation and removal of the daughter activity. The daughter activity is continuously replenished by the decaying parent. Since the parent half-life (66 h) is significantly longer than that of the daughter (6 h), the generator can be used for more than 1 week.

1.2.3

Interactions of Radiation with Matter

1.2.3.1

Elastic and Inelastic Interactions

Radiation interacts with matter by either elastic or inelastic interactions. In an elastic interaction, the incident radiation is scattered in a different direction but does not lose energy. In contrast, in an inelastic interaction, energy is lost. Photons (X- and γ -rays) are emitted as a result of radioactive decay and are referred to as ionizing radiation; such radiations are sufficiently energetic that they can ionize atoms of a stopping medium, ejecting an electron, and producing an ion pair consisting of a free negative electron and a positive ion.

1.2.3.2

Photon (X- and γ -ray) Interactions

Ionizing radiations (i.e., X- and γ -rays) undergo inelastic interactions by one of several mechanisms: the photoelectric effect, Compton scatter, pair production, and photodisintegration. Pair production, in which an X- or γ -ray interacts with an atomic nucleus and produces a positron-electron pair, has an energy threshold (to account for the combined rest mass energies of the positron and electron created) of 1.022 MeV. Photodisintegration, in which an X- or γ -ray interacts with and fragments the nucleus, has an even higher energy threshold of at least several MeV. Pair production and photodisintegration are therefore not energetically possible for the range of relatively low-energy X- and γ -rays encountered in nuclear medicine and will not be considered further. In the photoelectric effect (Fig. 1.5a), the X- or γ -ray energy is completely transferred to an orbital electron in an atom of the stopping medium, some of the energy used to eject the electron from the atom and the remainder providing kinetic energy to the electron. Usually an inner shell electron is ejected from the atom and the inner shell vacancy is filled with an outer shell electron, the energy difference released as an X-ray. In Compton scatter (Fig. 1.5b), only a portion of the incident photon's energy is transferred to an orbital electron, which is likewise ejected from the atom. The scattered photon's energy is therefore less than that of the incident photon and it travels in a different direction. The *relative* probability of the photoelectric effect increases as the incident photon energy, E_γ , decreases and the effective atomic number, Z_{eff} of the

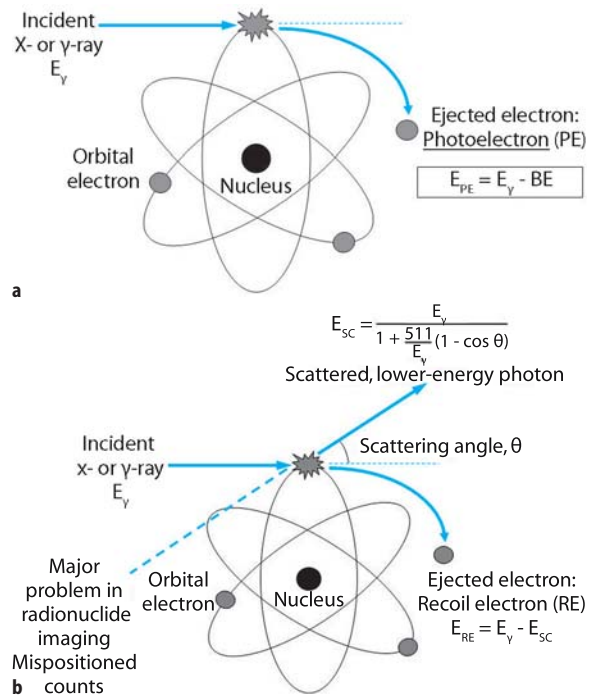


Fig. 1.5. Interactions of X- and γ -rays in matter in the energy range encountered in nuclear medicine. **a** In the photoelectric effect, the energy, E_{PE} , of the ejected electron, termed the photoelectron (PE), is $E_\gamma - BE$ where E_γ is the energy of the incident photon and BE is the binding energy of that electron in the atom. Note that the incident photon disappears completely. **b** In Compton scatter, the photon does not disappear but is scattered with a lower energy (in keV), E_{SC} ; E_{SC} is a function of the energy (in keV) of the incident photon, E_γ , and the scattering angle, θ , as indicated by the equation shown. The energy of the recoil electron (RE), E_{RE} , is therefore $E_\gamma - E_{SC}$. Compton scatter generally involves outer-shell orbital electrons with binding energies, BEs, negligibly small compared to typical values of E_γ and E_{SC} ; the binding energy, BE, is therefore ignored in calculating the energy of the recoil electron. (Adapted from Zanzonico 2002 in the "Further Reading" list)

stopping medium increases (i.e., proportional to E^3/Z^3). Conversely, the *relative* probability of Compton scatter increases slightly as E_γ increases and Z_{eff} decreases. For X- and γ -ray energies typically encountered in nuclear medicine, the predominant mode of interaction in soft tissue (low Z) is Compton scatter and in scintillation detectors (such as thallium-doped sodium iodide, NaI(Tl)) (high Z) the photoelectric effect.

The mathematics of X- and γ -ray attenuation follows an exponential relationship and is similar in form to the mathematics of radioactive decay. For an attenuating medium of thickness x this relationship is:

$$I(x) = I(0)e^{-\mu x} \quad (1.10)$$

where μ = the linear attenuation coefficient
 = the fraction of photons attenuated per unit thickness of stopping material (e.g., in cm^{-1}).

- $I(x)$ = the photon intensity transmitted through a thickness x of stopping material, and
 $I(0)$ = the incident photon intensity.

The linear attenuation coefficient, μ , is a property of both the photon energy and the stopping material: μ increases (i.e., photons become less penetrating) for low photon energy and low mass density.

In addition to the linear attenuation coefficient, μ , other quantities express the attenuation of X- and γ -rays in an attenuating material: the half-value layer, HVL (or half-value thickness, HVT), which is the thickness required to reduce the photon intensity by one-half; and the mean free path, MFP, is the thickness a photon travels, on average, before interacting. The linear attenuation coefficient, μ , half-value layer, HVL, and mean free path, MFP, are mathematically related as follows:

$$\text{or: } \mu = 0.693/\text{HVL} \quad (1.11)$$

$$\text{HVL} = 0.693/\mu \quad (1.12)$$

$$\text{MFP} = 1.44 \text{ HVL} \quad (1.14)$$

Combining Eqs. 10 and 11 yields the most common form of the attenuation equation:

$$I(x) = I(0)e^{-0.693/\text{HVL} \cdot x} \quad (1.14)$$

Note that when the absorber thickness, x , is equal the HVL, the equation correctly predicts that 50% of the incoming radiation is stopped by the absorber. Another convenient term used when dealing with larger amounts of attenuation is the tenth value layer (TVL) or (Tenth Value Thickness), referring to a thickness which permits only 10% of the incident radiation to penetrate a medium. The TVL is related to the HVL by $\text{TVL} = 3.32 \text{ HVL}$.

1.2.3.3

Particulate-Radiation Interactions

Particulate radiations (i.e., β -rays, Auger and conversion electrons) interact with matter by one of two mechanisms: collisional interactions and radioactive interactions. Collisional interactions are somewhat analogous to Compton scatter: an incident β -ray or electron “collides” with and transfers sufficient energy to an orbital electron to eject it from the atom and, in the process, is scattered with a lower energy. In radioactive interactions, on the other hand, the β -ray or electron penetrates the electron “cloud” and reaches and interacts with the atomic nucleus. However, because of the large mass disparity (of the order of a thousand-fold) between electrons and nucleons, the energy lost by the incident β -ray or electron in this interaction appears as X-rays, or *Bremsstrahlung* (German for “brake radiation”), rather than as kinetic energy of the nucleus. *Bremsstrahlung* exhibits a broad energy spectrum, with X-ray energies ranging from zero to a maximum

value equal to the energy of the incident particle. For the range of β -ray and electron energies (up to approximately several hundred keV) typically encountered in nuclear medicine, the predominant type of interaction in soft tissue (which has a relatively low Z_{eff}) is overwhelmingly collisional interactions, with less than 1% of the interactions attributable to radioactive interactions.

There is a large disparity in penetrabilities of photon versus particulate radiations. The X- and γ -rays typically encountered in nuclear medicine have energies of the order of several hundred keV and thus a significant proportion of such radiations can penetrate soft-tissue thicknesses of the order of 10 cm or more. As a result, X- and γ -ray-emitting radionuclides in vivo can be detected and imaged. In contrast, β -rays and electrons are non-penetrating radiations and β -ray and electrons typically encountered in nuclear medicine have ranges in soft tissue of the order of only 1 mm or less. Thus, β -ray- and electron-emitting radionuclides in vivo cannot be detected and imaged non-invasively. In addition, since all their energy is deposited locally, particulate radiation produces a much higher local radiation burden, which makes these radionuclides well suited for radionuclide therapy.

1.3

Radiation Detection and Measurement

1.3.1

Statistical Considerations

Radioactive decay is a random process and therefore random fluctuations will occur in the measured counts or count rates arising from decay of radioactivity. Such random fluctuations complicate the accurate detection, measurement, and imaging of radioactivity. If a detector were used to repeatedly measure the counts or count rates from a given activity, slightly different values would be obtained from measurement to measurement. If an average of N counts is obtained, the standard deviation, σ , of the number of counts is:

$$\sigma = \sqrt{N} \quad (1.15)$$

and the percent standard deviation (or “noise”), $\% \sigma$, is:

$$\% \sigma = \frac{100\%}{\sqrt{N}} \quad (1.16)$$

As an example, if a sample count were 100, the $\% \sigma = 10\%$. Using the laws of a normal distribution we can interpret this as: if we counted a radioactive sample many times, two-thirds of the time the count would be within 10% of the true value. If, on the other hand, we counted for a longer time and measured 1,000 counts, the $\% \sigma = 3.3\%$; two-thirds of the time the count would be within 3.3% of the true value. Measuring for longer

times and obtaining more counts thus produces less random variation in the measurement and the measured value is closer to the true value. This principle applies to the counting of radioactive samples or to planar imaging of radioactivity [i.e., to the counts per unit picture element (or pixel) in a planar image]. In other words, the more counts in an image, the better the statistical accuracy of the image.

1.3.2

Radiation Detector Performance

Radiation detectors may be quantitatively characterized by many different performance parameters. Among the most important of these, however, are sensitivity (or efficiency), energy resolution, and, for devices which localize (image) as well as count radiation, spatial resolution and uniformity.

Sensitivity (or efficiency) is the detected count rate per unit activity. Because the count rate detected from a given activity is highly dependent on the source-detector geometry and intervening absorbing media, characterization of sensitivity can be ambiguous. There are two methods for evaluating sensitivity: geometric sensitivity and intrinsic sensitivity. Geometric sensitivity is the fraction of emitted radiations which intersect, or strike, the detector, that is, the fraction of the total solid angle subtended by the detector. It is therefore directly proportional to the radiation-sensitive detector area and, for a point source, inversely proportional to the square of the source-detector distance. Intrinsic sensitivity is the fraction of radiations intersecting the detector which is stopped within the detector. Intrinsic sensitivity is directly related to the detector thickness, effective atomic number, and mass density and decreases with increasing photon energy, since higher-energy photons are more penetrating and are more likely to pass through a detector without interacting.

Characteristic X-rays and γ -rays are emitted from radioactively decaying atoms with well-defined discrete energies. Due to photon scatter from intervening material (i.e., a patient) and even in the absence of scatter, output electrical pulses from absorption of these radiations will appear to originate from a range of energies. This reflects a limitation of the detector. For this reason, many radiation detectors employ some sort of energy-selective counting: an energy range, or window, is selected such that radiations are counted only if their detected energies lie within that range. Commonly (at least for scintillation detectors such as gamma cameras; see below), a so-called “20% photopeak energy window,” $E_\gamma \pm 10\%$ (e.g., 126–154 keV for the 140-keV γ -ray of ^{99m}Tc) is employed, where E_γ is the primary (referred to as the photopeak) energy of the radiation. For such energy-selective counting, overall sensitivity appears to increase as the photopeak energy window is

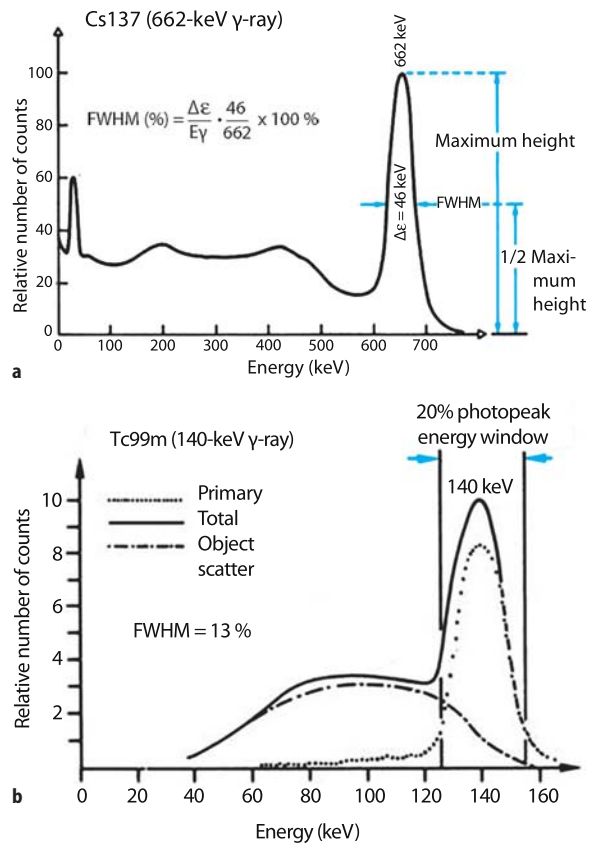


Fig. 1.6. **a** Energy spectrum for the 662-keV γ -rays emitted by ^{137}Cs , illustrating the definition of energy resolution as the % full-width half-maximum (FWHM) of the photopeak energy, E_γ . **b** Energy spectrum for the 140-keV γ -rays emitted by ^{99m}Tc , illustrating the contributions of primary (unscattered) and scattered radiation counts. In **a** and **b**, the energy spectra were obtained with a thallium-doped sodium iodide [NaI(Tl)] scintillation detector (see text). (Adapted from Cherry et al. 2003 in the “Further Reading” list)

widened. However, this results in acceptance of more scattered as well as primary (i.e., unscattered) radiations. *Energy resolution* quantifies the ability of a detector to separate, or discriminate, radiations of different energies. As illustrated in Fig. 1.6a, energy resolution is generally specified as the full-width at half-maximum height ($\text{FWHM} = \Delta E$) expressed as a percentage of the photopeak energy (E_γ) of the bell-shaped photopeak,

$$\text{FWHM (\%)} = \frac{\Delta E}{E_\gamma} 100\%.$$

The importance of energy resolution lies in scatter rejection, particularly for imaging detectors. Radiation loses energy when scattered in the patient and the lower-energy scattered – and therefore mispositioned – radiations may therefore be discriminated from the primary radiations. However, the finite energy resolution of radiation detectors (i.e., the width of the photopeak in the energy spectrum) means that there will be overlap of scattered

and primary radiations, as illustrated in Fig. 1.6b. For systems with superior energy resolution (i.e., the FWHM (%) decreases and the photopeak becomes narrower), the separation of primary and scattered radiations permits scattered radiation to be eliminated while accepting more counts corresponding to primary radiation.

For detectors such as gamma cameras where radiation is localized (imaged) as well as detected and counted, *spatial resolution* is a critical performance parameter. It reflects the ability of the detector to accurately determine the location of a source or, similarly, the ability to visualize two closely spaced point sources. This is usually measured by imaging a point source and examining the spread of the image on the detector. The detector's spatial resolution can then be expressed as the full-width at half-maximum height (FWHM) of this point (or line) spread function. Spatial resolution generally worsens with increasing source-to-detector distance. There is a trade-off between sensitivity and resolution: they are inversely related: sensitivity is reduced as spatial resolution improves and spatial resolution is degraded as sensitivity increases.

Uniformity is likewise a critical parameter of gamma cameras and other imaging devices. In principle, a uniform source of radioactivity (i.e., usually a large disk with ^{57}Co uniformly imbedded in plastic) should yield a uniform image [i.e., an image in which the counts per unit picture element (or pixel) is constant over the entire image]. In practice, this is never achieved – even if one discounts the effects of count statistics (noise) – because of inevitable point-to-point variations in sensitivity of an imaging detector. Uniformity (actually, the deviation from uniformity) may be expressed by a quantity known as the “integral uniformity” (IU):

$$\text{IU} = \frac{\text{Maximal counts per pixel} - \text{Minimum counts per pixel}}{\text{Maximal counts per pixel} + \text{Minimum counts per pixel}} \times 100\% \quad (1.17)$$

To reliably estimate the IU, a very-high-count image (e.g., a 15-million count image for a gamma camera) of a uniform source minimizes the quantitative effect of count statistics (noise). Acceptable uniformity is $< 3.5\%$. A second more important parameter widely used to characterize uniformity (specifically, gamma camera uniformity) is the so-called “differential uniformity” (DU), the maximum value of the expression on the right side of Eq. 1.17 determined for every five-pixel segment in every row and column of a uniform-source image.

1.3.3

Basic Design and Operating Principles of Radiation Detectors

Radiation detectors are generally characterized as either scintillation or ionization detectors (Fig. 1.7). In

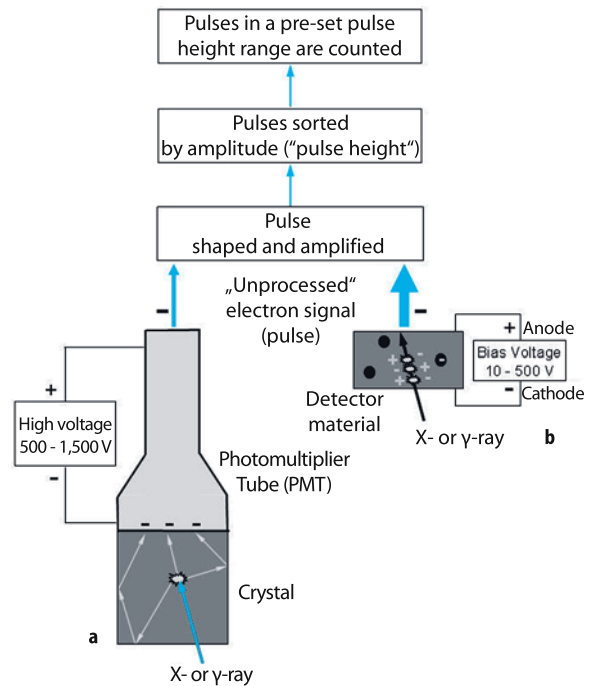


Fig. 1.7. The basic design and operating principle of **a** scintillation and **b** ionization detectors

scintillation detectors, visible light is produced as radiation exits atoms of a crystal and converted to an electronic signal, or pulse, and amplified by the photomultiplier tube (PMT). In ionization detectors, free electrons, produced as radiation ionizes a stopping material, are collected to produce an electronic signal.

1.3.4

Ionization Detectors

Detector materials in the most common ionization detectors are gaseous and such detectors are therefore often known as “gas-filled detectors.” See design of gas detectors in Fig. 1.7. The two most important gas ionization detectors for nuclear medicine are dose calibrators and Geiger counters. The principal difference among such detectors is the magnitude of the bias voltage between the anode and cathode, as indicated in Fig. 1.8 and Table 1.3. At a bias voltage of 300 V, all of the electrons produced directly by ionization of the detector material by an incident radiation X- or gamma-ray are collected at the anode and produce a fixed detector signal per gamma-ray. In the 300- to 600-V range the overall signal is equivalent to the primary number of electrons and is therefore proportional to the energy of the incident radiation. Dose calibrators operate in this range and are used to assay radiopharmaceutical activities before injecting patients. The relatively low sensitivity of such devices is not a major disadvantage, as ra-

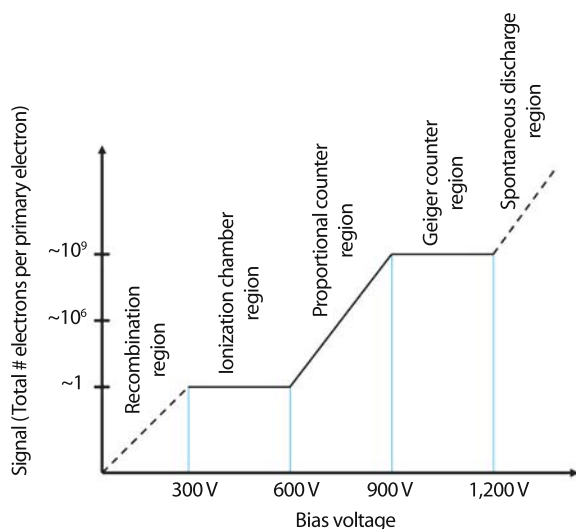


Fig. 1.8. The signal (expressed as the amplification factor, that is, the total number of electrons per primary electron produced in the detector material) as a function of the bias voltage for gas-filled ionization detectors. The principal difference among such detectors is the magnitude of the bias voltage between the anode and cathode. The amplification factors and the voltages shown are approximate

Table 1.3. Properties of gas-filled ionization detectors

	Ionization detector	Proportional counter	Geiger counter
Bias-voltage operating range	300–600 V	600–900 V	900, 1,200 V
Response stable with respect to voltage? ^a	Yes	No	Yes
Sensitivity ^b	Low	Intermediate	High
Capable of energy discrimination?	Yes	Yes	No
Applications	Dose calibrator	Research	Survey meter

^a Stability with respect to the bias voltage corresponds to a constant signal over the respective detector's operating voltage range. In contrast to ionization detectors and Geiger counters, proportional counters are unstable with respect to the bias voltage and thus require specialized, highly stable voltage sources for constancy of response

^b The sensitivity of a detector is related to its amplification factor (see Fig. 1.7)

^c If the total number of electrons comprising the signal is proportional to the number of electrons directly produced by the incident radiation and therefore proportional to its energy, as in ionization detectors and proportional counters, radiations of different energies can be discriminated (i.e., separated) on the basis of the signal amplitude

diopharmaceutical activities are typically rather large (i.e., in the μCi to mCi range). Energy discrimination is usually achieved by the use of precalibrated amplifiers,

one for each radionuclide. Ionization chambers operating at bias voltages in the 900- to 1,200-V range are “Geiger counters” (or “Geiger-Müller” or “GM”). In contrast to ionization chambers the Geiger counter output signal is independent of the number of primary electrons and the energy of the incident radiation. The output is referred to as an “all-or-nothing” response, meaning that if an incoming photon has sufficient energy the Geiger counter will register the count. Geiger counters, because of their high sensitivity and stability with respect to voltage (allowing the use of a portable power supply such as an ordinary battery), are well suited and widely used as survey meters for ambient radiation levels and radioactive contamination. For survey meters, sensitivity, and not energy discrimination, is critical.

1.3.5

Scintillation Detectors

In scintillation detectors (Fig. 9a), radiation interacts with and deposits energy in a scintillator, most commonly a crystalline solid such as thallium-doped sodium iodide [NaI(Tl)]. The radiation energy thus deposited is converted to visible light. Because the light is emitted isotropically (i.e., in all directions), the inner surface of the light-tight crystal housing is coated with a reflective material so that light emitted toward the sides and front of the crystal are reflected back toward a PMT (Fig. 1.9b) (gamma cameras have 37–105 PMTs per detector); this maximizes the amount of light collected and therefore the overall sensitivity of the detector. In addition, this insures that the amount of light detected is proportional to the energy of the absorbed photon. Interposed between the back of the crystal and the entrance window of the PMT is the light pipe, nowadays simply a thin layer of transparent optical gel. The light pipe optically couples the crystal to the PMT and thus maximizes the transmission (>90%) of the light signal from the crystal into the PMT.

The operation of the photomultiplier tube is as follows: Coated on the inner surface of the PMT is the photocathode. When struck by the light from the crystal, the photocathode, which is at ground (i.e., 0 V), emits electrons. Immediately beyond the photocathode is the focusing grid, maintained at a relatively low positive voltage of the order of 10 V. Electrons pass through the focusing grid; they are attracted by a relatively large positive voltage, ~ 300 V, on the first of a series of small metallic elements called dynodes. The resulting high-speed impact of each electron results in the ejection from the dynode surface of an average of three electrons. The electrons thus ejected are then attracted by the even larger positive voltage, ~ 400 V, on the second dynode. The impact of these electrons into the second

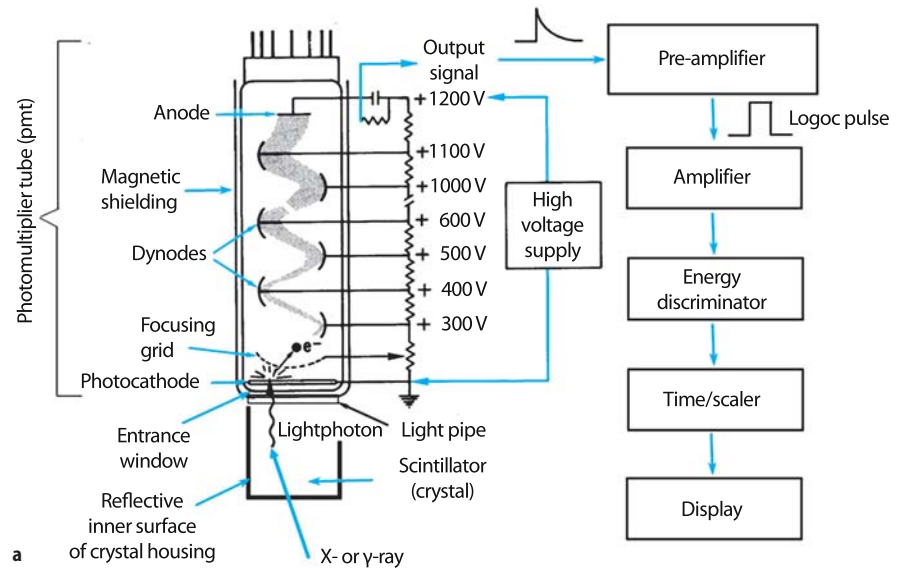


Fig. 1.9. **a** The basic design and operating principle of PMTs and scintillation detectors. **b** Photographs of PMTs. The PMTs circled are typical of those used in gamma cameras



dynode surface ejects an additional three electrons for each incident electron. Typically, a PMT has 10–12 such dynodes (or stages) each ~ 100 V more positive than the preceding dynode resulting in an overall electron amplification factor of 3^{10} to 3^{12} for the entire PMT. At the last anode an output signal is generated. The irregularly shaped PMT output signal is then shaped by a pre-amplifier and further amplified into a logic pulse that can be electronically manipulated. The resulting electrical pulses, whose amplitudes (or “heights”) are proportional to the number of electrons produced at the PMT photocathode, are therefore also proportional to the energy of the incident radiation. These pulses can then be sorted according to their respective heights by an energy discriminator (also known as a pulse height analyzer) and those pulses with a pulse height (i.e., energy) within the preset photopeak energy window (Fig. 1.9a) are counted by the timer/scaler.

In addition to their widespread use in gamma cam-

eras and SPECT and PET scanners, scintillation detectors are used in well counters, intraoperative probes, and organ (“thyroid”) uptake probes.

1.4 Nuclear Medicine Instrumentation

1.4.1 Intraoperative Probes

Intraoperative probes (Fig. 1.10), small, handheld counting devices, are now widely used in the management of cancer: most commonly, to more expeditiously identify and localize sentinel lymph nodes and thereby reduce the need for more extensive surgery; in addition, to identify and localize visually occult disease at surgery following systemic administration of a radiolabeled antibody or other tumor-avid radiotracer. [Although intraoperative probes have been used almost

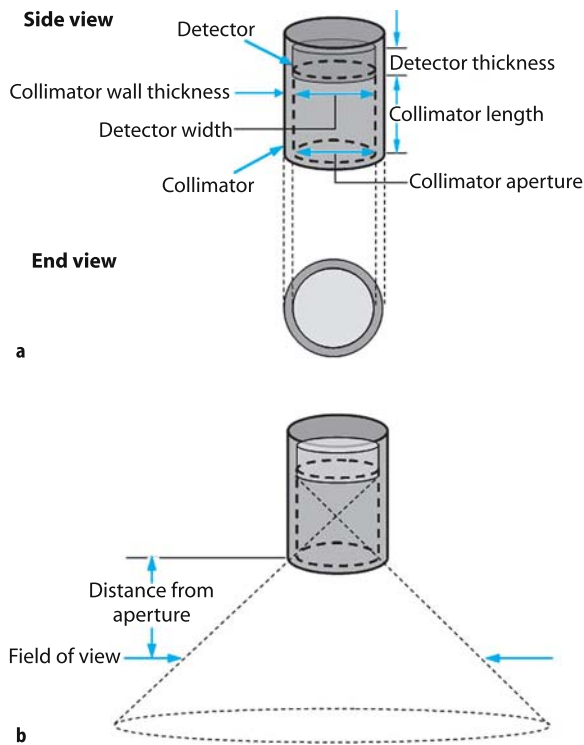


Fig. 1.10. **a** Basic design of a gamma probe collimator. The collimator may be thought of as an extension of the detector shielding in the forward direction, that is, beyond the detector face in the desired counting direction. A collimator may be characterized by its aperture (generally, but not necessarily, equal to the width of the detector), its length, and its wall thickness. **b** The probe's FOV, that is, the area of tissue from which unscattered X- or γ -rays may reach the detector, increases with increasing distance from the collimator aperture. The volume of tissue from which unscattered X- or γ -rays may reach the detector is thus a three-dimensional cone diverging outward from the collimator (the dotted line). (Adapted from Zanzonico 2002 in the "Further Reading" list)

exclusively for counting X- and γ -rays, beta (electron and positron) probes constructed with plastic scintillators have also been developed. As well, small field-of-view intraoperative gamma cameras, with up to 12.5 cm field of view, have recently become available to simplify and improve the accuracy for localization of sentinel nodes and tumors.] Intraoperative gamma probes are available with either scintillation or semiconductor (ionization) detectors. Scintillation detector-based probes have the advantages of relatively low cost and high sensitivity (mainly because of their greater thickness, ~ 10 mm, versus only ~ 1 mm in ionization detectors), especially for medium- to high-energy photons. Disadvantages include bulkiness and relatively poor energy resolution and scatter rejection relative to semiconductor based probes. In some scintillation-detector intraoperative probes, the light signal from the crystal is guided to a remote PMT through a flexible fiberoptic cable, allowing the probe assembly to be made

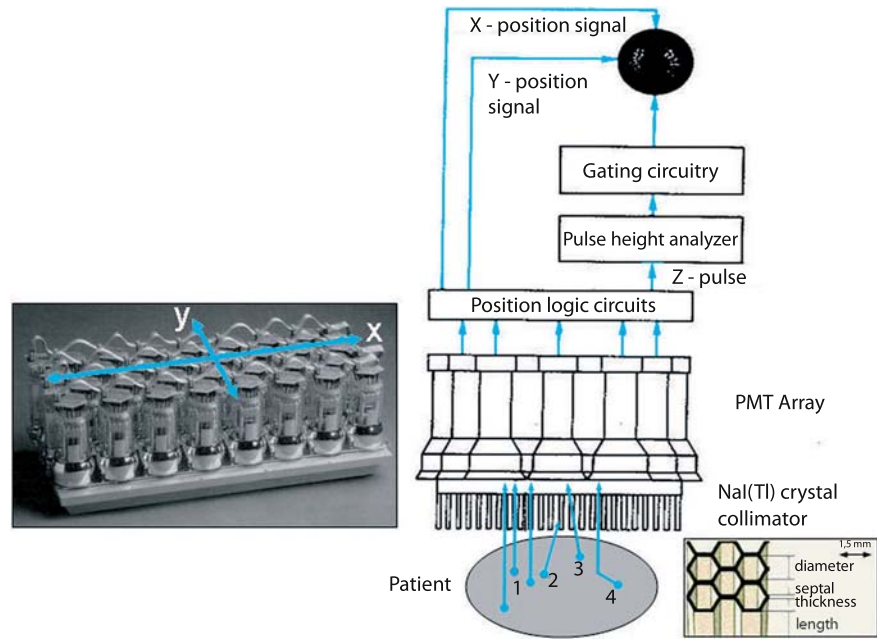
relatively light and compact and more like a surgical instrument, but the significant loss of light in the long cable makes it more difficult to separate scatter from direct gamma rays. On the other hand, semiconductor-based probes are compact and have excellent energy resolution and scatter rejection. To minimize an internal signal problem which degrades the energy resolution, semiconductor detectors are made relatively thin (only ~ 1 mm), but at the cost of lower intrinsic sensitivity. The main disadvantage of semiconductor detectors remains their limited thickness and resulting lower sensitivity, especially for medium- to high-energy X- and γ -rays. Nonetheless, while scintillation detectors can be made thicker and therefore more sensitive, semiconductor detectors produce more electrons per X- and γ -ray stopped and therefore have superior energy resolution. To date, the few clinical studies directly comparing scintillation and semiconductor intraoperative probes have not provided a clear choice between the two types of probes.

1.4.2

Organ Uptake Probes

Historically, organ uptake probes have been used almost exclusively for measuring thyroid uptakes and are thus generally known as "thyroid" uptake probes. Thyroid uptake (i.e., the decay-corrected percent of administered activity in the thyroid) can be measured following oral administration of radioiodide ($5 - 10 \mu\text{Ci}$ of ^{131}I in liquid or capsule form or $100 - 200 \mu\text{Ci}$ of ^{123}I in capsule form) or, less commonly, $^{99\text{m}}\text{Tc}$ -pertechnetate ($2 - 10 \text{mCi}$). The uptake probe is a radionuclide counting system consisting of a wide-aperture, diverging collimator, a NaI(Tl) crystal (typically ~ 5 cm thick by ~ 5 cm in diameter), a photomultiplier tube, a pre-amplifier, an amplifier, an energy discriminator (i.e., an energy window), and a gantry (stand). Commercially available thyroid uptake probes are generally supplied as integrated, computerized systems with automated data acquisition and processing capabilities, yielding results directly in terms of percent uptake. Each measurement of thyroid uptake generally includes the following: ambient (i.e., "room") background, a "thigh" background (measured over the patient's thigh and designed to account for the count contribution of extra-thyroidal neck activity), thyroid (i.e., neck) activity, and a standard (counted in a Lucite neck phantom simulating the thyroid/neck anatomy) activity. By including measurement of a standard activity with each uptake determination, precise corrections for radioactive decay and day-to-day variation in system sensitivity are automatic. (Alternatively, one may measure the administered activity itself in a phantom immediately prior to patient administration and then correct for radioactive decay when comparing with subsequent thy-

Fig. 1.11. Basic design of a gamma camera, consisting of a multi-hole collimator, a thin large-area NaI(Tl) crystal, a two-dimensional array of PMTs and associated electronics (high-voltage power supply, pre-amplifier, and amplifier), position logic circuitry, energy discriminator, and image display. Note that there are actually two position logic circuits – for the determination separately of the *x*- and *y*-positions of the scintillation within the crystal. Note further that the output signal from each PMT is actually split into three parts, one (the *z* pulse) for the determination of the energy of the incident radiation as well as one each for the determination of its *x*- and *y*-positions. The *left inset* shows a photograph of the two-dimensional PMT array backing the crystal in a typical rectangular field-of-view gamma camera. The *right inset* shows a drawing of a portion of a parallel-hole collimator, identifying the dimensions – aperture diameter, septal thickness, and septal length – of such a collimator. The “desirable” events (arrows labeled “1”) are unscattered (i.e., photopeak) photons traveling in a direction parallel or nearly parallel to the axes of the apertures and thus yielding correctly positioned counts in the gamma camera image. “Undesirable” events include: scattered as well as unscattered photons traveling in a direction oblique to the axes of the apertures (2) and thus eliminated by attenuation by one or more collimator septa; septal penetration (3), that is, unscattered photons traveling in a direction oblique to the axes of the apertures yet passing through the septa and yielding mis-positioned counts; scatter (4), that is, photons undergoing Compton scatter within the patient and either eliminated by energy discrimination or not eliminated and yielding mis-positioned counts (Fig. 1.6b). (Adapted from Cherry et al. 2003 in the “Further Reading” list)



roid uptake measurements.) The standard consists of a solution containing a known amount of activity. The thyroid uptake is then calculated by subtracting room and thigh background counts from the thyroid measured activity and comparing to the phantom activity (which would represent 100% uptake).

Thyroid uptake measurements can also be performed from planar scintigraphic images of the neck and of a standard (i.e., phantom) acquired with a gamma camera fitted with a parallel-hole collimator.

1.4.3 Gamma Cameras

Developed in the late 1950s by Hal Anger, the gamma camera (Fig. 1.11), also known as the scintillation or Anger camera, has become the predominant imaging device in nuclear medicine – mainly because its large detector area allows simultaneous and therefore rapid data acquisition over a large area of the body. Gamma camera crystals vary in thickness from 1/4” (yielding the best spatial resolution but lowest sensitivity) to 1” (yielding the highest sensitivity but coarsest resolution and mostly used for imaging the 511-keV photons of

¹⁸F), with 3/8”-thick crystals providing the optimum balance between sensitivity and resolution and remaining the most widely used for general gamma camera imaging. About 95% of the 140-keV photons from ⁹⁹Tc are absorbed in a 3/8” crystal. Gamma camera NaI(Tl) crystals are nowadays most commonly rectangular in shape and ~50×60 cm in area.

The gamma camera collimator, almost always composed of lead, “directionalizes” the incoming radiation: any radiation traveling at an oblique angle to the axes of the holes (apertures) will strike the lead walls (septa) between the holes and not reach the crystal, thereby allowing only radiation traveling perpendicular to the crystal surface to pass through the apertures and contribute counts to the resulting image. Of course, a certain fraction of photons striking the septa will nonetheless pass through them and reach the crystal (about 5%); this phenomenon, which degrades image quality, is known as septal penetration. Almost all collimators are parallel hole collimators, in which the apertures and septa are parallel to one another. In addition, single-aperture pinhole collimators, most commonly used for thyroid imaging because of their pronounced magnifying effect, are available as well. Pin-hole collima-

tors, however, suffer from geometric distortion, that is, image magnification varies with both distance and lateral distance from the center of field.

Gamma camera collimators are “rated” with respect to photon energy and resolution/sensitivity. Low-energy, or “technetium,” collimators, referred to as “low energy all purpose” collimators (LEAP) or “low energy high resolution” collimators (LEHR), are designed to image radionuclides emitting X- and γ -rays less than 200 keV in energy, including, most notably, ^{99m}Tc (photopeak energy: 140 keV) as well as ^{201}Tl (68–80 keV), ^{123}I (159 keV), and ^{57}Co (124 keV). Medium-energy, or “gallium,” collimators are designed for radionuclides emitting X- and γ -rays 200–300 keV in energy, including ^{67}Ga (93, 185, and 300 keV) as well as ^{111}In (172 and 247 keV). High-energy, or “iodine,” collimators are designed to image radionuclides emitting X- and γ -rays greater than 300 keV in energy, including ^{131}I (364 keV). Today, many departments no longer have a high energy collimator and use a medium energy collimator for imaging ^{131}I , accepting the increased septal penetration but achieving a better image quality and improved sensitivity, which is important when imaging the low ^{131}I activity in patient studies. In progressing from low- to medium- to high-energy collimation, the collimators are made longer and the septa thicker in order to interpose more lead between the patient and the crystal and to thereby maintain septal penetration (i.e., the percent of counts in an image attributable to photons that penetrate septa) at or below an acceptably low level, typically set at 5%. This, in turn, reduces the overall fraction of emitted X- and γ -rays reaching the crystal. To compensate, at least in part, for the resulting lower sensitivity, the apertures are typically made wider in progressing from low- to medium- to high-energy collimators. This, however, degrades spatial resolution. Overall, therefore, gamma camera images are progressively poorer in quality for radionuclides emitting low- versus medium- versus high-energy X- and γ -rays because of a combination of increased septal penetration with increasing photon energy, lower sensitivity because of the longer collimation, and coarser resolution because of the wider apertures. For each energy rating, collimators may also be rated as “general-purpose” (or “all-purpose”), “high-resolution,” or “high-sensitivity.” High-resolution collimators have narrower apertures (and therefore lower sensitivity) and high-sensitivity collimators have wider apertures (and therefore coarser resolution), respectively, than general-purpose collimators. Finally, in instances where a radionuclide emits each of a number of photons in significant amounts, it is the highest-energy photon which dictates the collimator to be used. For example, a medium-energy collimator must still be used to image ^{67}Ga (photon energies: 93, 185, and 300 keV) even if only the two lower-energy (i.e., the 93- and 185-keV) photons are used for

imaging. (For some older systems, only two, rather than three, photon energies can be imaged simultaneously.)

Once the incident radiation passes through the collimator aperture, it strikes and may produce a scintillation within the crystal. The resulting light signal is spread out among the PMTs in a two-dimensional array on the back of the crystal, the intensity varying inversely with the distance between the scintillation and the respective PMT: the further the PMT is from the scintillation, the less light it receives and the smaller its output pulse. This inverse linear relationship is the basis of the Anger position logic circuitry for determining the precise position of a scintillation within the crystal. In the older gamma cameras, the x - and y -coordinates were calculated by analog circuitry, that is, using matrices of resistors. In newer models, this is done by digitizing the output signal from each PMT with an analog-to-digital converter (ADC) and using digital electronics.

1.4.4

Tomographic Scanners

1.4.4.1

Introduction

A “tomogram” is literally a picture of a slice. Tomography may be characterized as either transmission or emission tomography depending on the origin of the radiation. In transmission tomography, X-rays are transmitted through the patient; in emission tomography, X- or γ -rays are emitted from within the patient. Emission tomography can be further characterized on the basis of the nature of the emitted radiation. Single photons, such as gamma-rays associated with isomeric transition and X-rays associated with electron capture or internal conversion, form the basis of single-photon emission computed tomography (SPECT). The two 511-keV annihilation photons simultaneously emitted following positron-electron annihilation and associated with positron emission form the basis of positron emission tomography (PET).

In computed tomography, the basic paradigm includes acquisition of images from multiple angles around a patient (multiple projections), correction of the acquired data for non-uniformity, and mathematical reconstruction of thin (several-millimeter thick) transverse tissue-section images. In both SPECT and PET, the reconstructed transverse-section images are essentially contiguous, with no inter-section gaps, and therefore the reconstructed three-dimensional array of volume elements, or voxels, may be rearranged at any angle relative to the longitudinal axis of the patient and thus yield coronal, sagittal, or oblique images. The principal advantage of tomography thus lies in its improved image contrast: by eliminating the count contri-

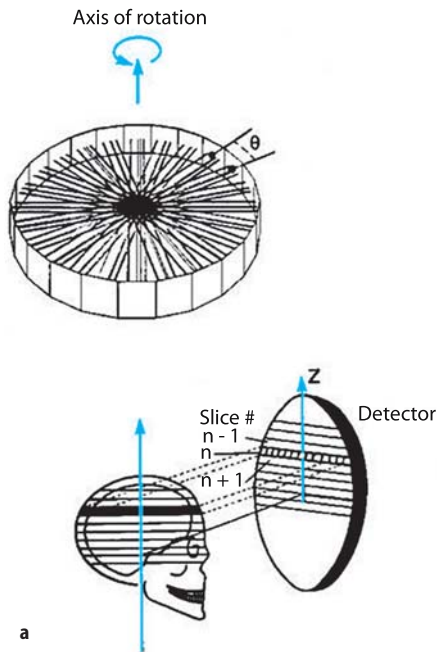


Fig. 1.12. **a** The basic data-acquisition paradigm in rotating gamma-camera SPECT. Photographs of modern dual-detector gamma cameras, with **b** the two detectors in opposed positions, as routinely used for a 360° rotation and general (non-cardiac) SPECT and **c** the two detectors perpendicular to each other, as routinely used for a 180° rotation and cardiac SPECT (from approximately right anterior oblique to left posterior oblique). The obvious advantage of such two-detector systems is that two projection images can be acquired simultaneously and the acquisition time therefore halved. (Adapted from Zanzonico 1995 in the “Further Reading” list)

bution from activities in tissues above and below the section of interest, the target (e.g., tumor)-to-background count ratio may dramatically improve.

1.4.4.2

SPECT Data Acquisition

Although there are many possible combinations of detector number, geometry, and motion that can acquire the necessary projection data, rotating gamma camera-based SPECT systems occasionally use one or three detectors but most commonly use two detectors. The raw data are acquired as a series of discrete planar images at multiple angles about the longitudinal axis of the patient (Fig. 1.12). The number of counts recorded in each projection-image pixel represents the ray sum, or line integral, of the sampling line perpendicular to and extending from the detector through the patient. The following are typical user-defined parameters: a 64×64 acquisition matrix with 180° rotation is routine for cardiac SPECT whereas a 128×128 acquisition matrix with a 360° rotation is common for non-cardiac SPECT.

1.4.4.3

PET Data Acquisition

PET is based on the annihilation coincidence detection (ACD) of the two co-linear (approximately 180° apart) 511-keV γ -rays resulting from the mutual annihilation of a positron and an electron (Fig. 1.13). Each time an annihilation photon is absorbed by a detector is referred to as a “single” event and the total count rate of individual annihilation photons is called the “singles count rate.” When both photons from an annihilation are absorbed simultaneously (in coincidence) in two opposing detectors, this triggers the coincidence circuit and a “true coincidence event” (“true”) is generated. The singles count rate in PET is typically much higher than the true count rate. The volume between the opposed coincidence detectors absorbing the two annihilation photons (the shaded area in Fig. 1.13a) is referred to as a “line of response (LOR).” LORs are thus defined electronically, and an important advantage of ACD is that a collimator is not required. As a result, the sensitivity of PET is two to three orders of magnitude higher than that of gamma camera imaging. As shown in Fig. 1.13b, modern PET scanners employ a series of rings of discrete, small-area

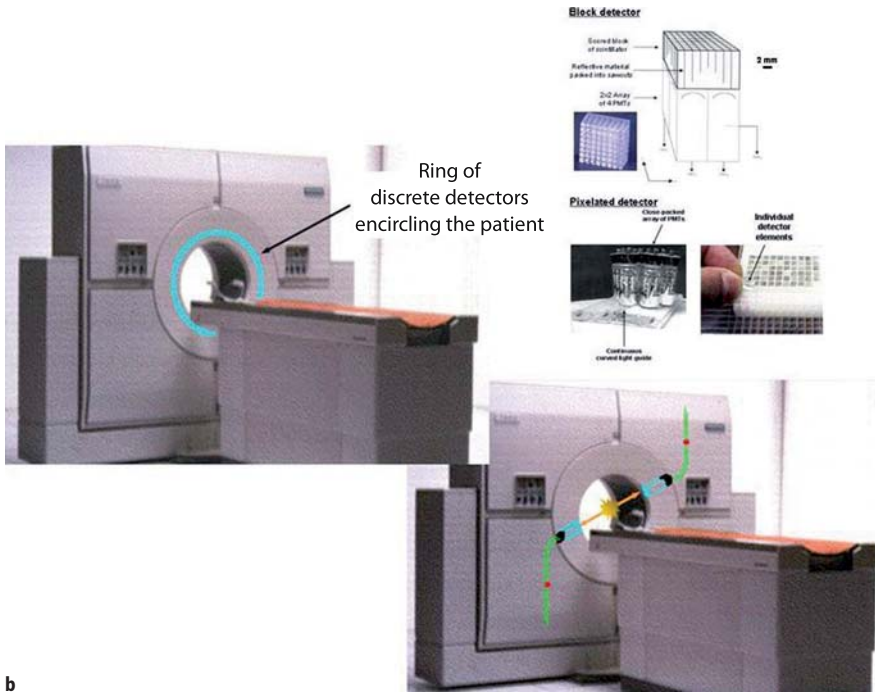
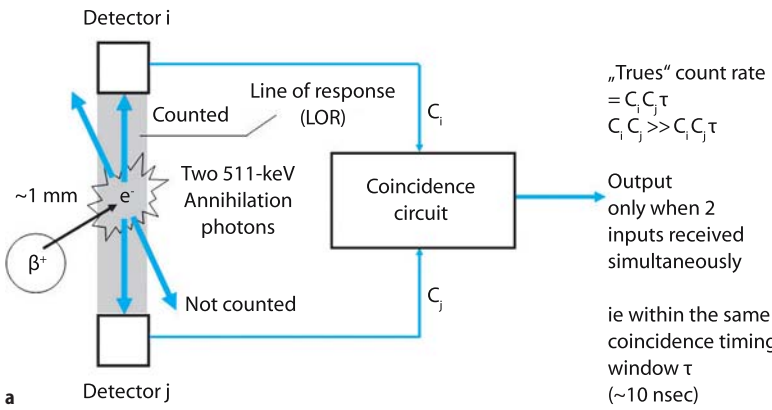


Fig. 1.13. a Annihilation coincidence detection (ACD) of the two opposed 511-keV γ -rays resulting from positron decay and positron-negatron annihilation. Note that the true coincidence (or “trues”) count rate, given by the product of the singles count rates, C_i and C_j , and the coincidence timing window, τ , is much less than C_i and C_j – the coincidence timing window, τ , is short (< 10 ns) to minimize the number of random coincidence events (Fig. 1.14), and most of the annihilation photons therefore do not produce coincidence events. **b** A photograph of a modern PET, illustrating one of a number of rings of discrete detectors encircling the patient (left-hand panel) and ACD of an annihilation photon by a pair of these detectors. In the insert are shown a block detector (top) and pixelated detectors (bottom) currently used in PET scanners. The block detector consists of a cubic piece of scintillator scored to variable depths into a two-dimensional array of detector elements, typically backed by a 2×2 array of position-sensitive PMTs. Pixelated detectors consist of individual scintillator detector elements backed by a continuous light guide and a close-packed array of PMTs. For both the block and pixelated detectors, the individual detectors elements are typically $\sim 2 \times 2$ mm in area. (Adapted from Zanzonico 2004 in the “Further Reading” list)

detectors (i.e., scored block detectors or pixelated detectors) encircling the patient and typically spanning a distance of 10–20 cm in the patient’s longitudinal direction. Thus, a whole-body PET scan will typically require data acquisition at six to seven discrete bed positions and subsequently merge or “knit”, the discrete images into a single whole-body image.

PET scintillation detectors typically have a rather coarse (up to 30%) energy resolution (compared to 8–9% for traditional gamma cameras) and therefore photons within a broad energy range (e.g., 250–650 keV) can be counted as valid annihilation γ -rays. Therefore, significant numbers of Compton-scattered annihilation γ -rays may be recorded as mis-positioned coincidence events. Since one or both may have been scattered, this creates a mispositioned event. Further, a true coincidence event is defined as a pair of an-

nihilation photons counted by the coincidence detectors within a finite time interval called the “coincidence timing window τ ,” typically 6–12 ns – mainly due to the finite time required for scintillation detectors to detect and register a radiation event. The coincidence window is needed to reject the significant fraction of singles events. However, two random events occurring within the coincidence window will be detected as a true event. In addition, the high number of events/s that can be detected in a system with no collimator means that two unrelated singles events may also be detected within the 6- to 12-ns window as a true event. The various events associated with ACD of positron-emitting radionuclides, including trues, randoms, scatter, and spurious coincidences or singles, are illustrated in Fig. 1.14.

PET ring scanners originally employed lead or tungsten walls, or septa, positioned between and extending

Fig. 1.14. The various events associated with ACD of positron-emitting radionuclides, illustrated for two opposed banks of coincidence detectors and assuming only one opposed pair of detectors are in coincidence. A true coincidence (“true”) is counted only when each of the two 511-keV annihilation γ -rays for a single positron-negatron annihilation are not scattered and are detected within the timing window τ of the two coincidence detectors. A random or accidental coincidence (“random”) is an inappropriately detected and positioned coincidence (the *dashed line*) which arises from two separate annihilations, with one γ -ray from each of the two annihilations detected within the timing window τ of the coincidence-detector pair. A scattered coincidence (“scatter”) is a mispositioned coincidence (the *dashed line*) resulting from a single annihilation, with one of the γ -rays undergoing a small-angle Compton scatter but retaining sufficient energy to fall within the 511-keV energy window. A spurious coincidence is an inappropriately detected and positioned coincidence (the *dashed line*) which arises from an annihilation and a cascade γ -ray, scattered or unscattered but having sufficient energy to fall within the 511-keV energy window. Spurious coincidences occur only for radionuclides which emit both positrons and high-energy prompt cascade γ -rays, that is, γ -rays with energies (either scattered or unscattered) lying within the 511-keV energy window. (Adapted from Cherry et al. 2003 in the “Further Reading” list)

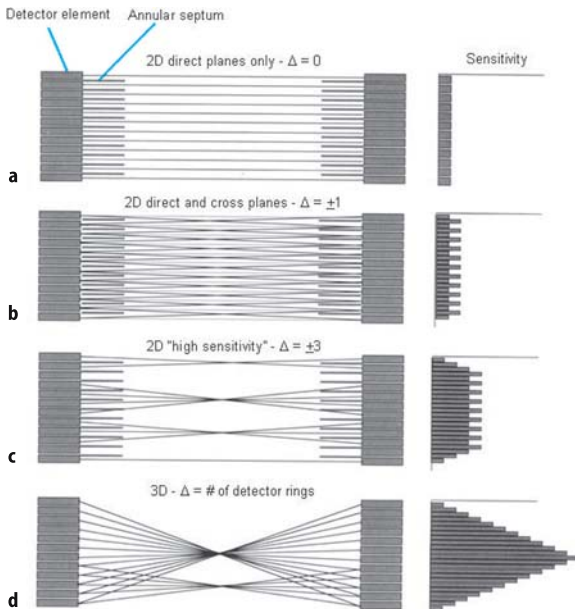
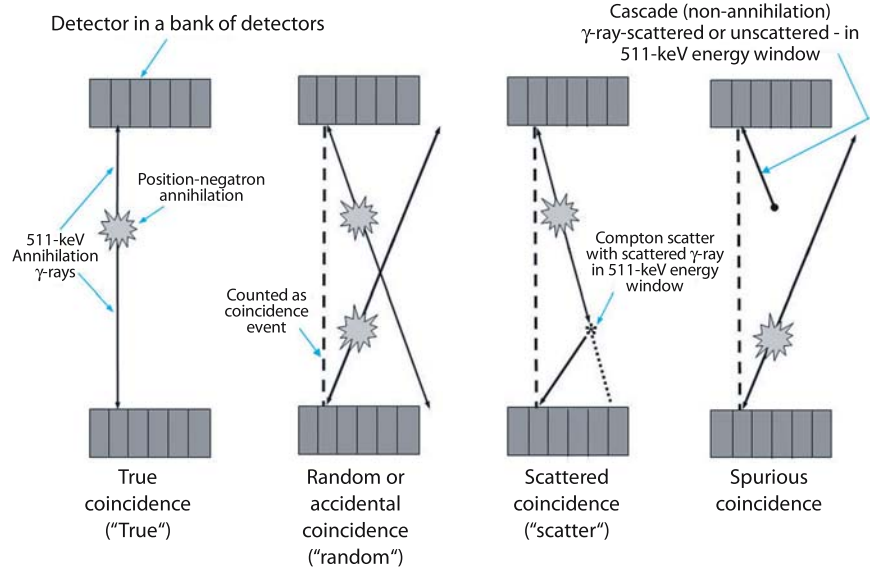


Fig. 1.15. Two-dimensional (2D) and three-dimensional (3D) PET data acquisition schemes (axial cross-sectional views of a multi-ring scanner) and the corresponding axial sensitivity profiles. **a–c** 2D data acquisition with a ring difference Δ of 0 (direct planes only), 1, and 3, respectively. **d** 3D (septa-less) data acquisition. The sensitivity profiles show the non-uniformity of response as a function of position along the axial FOV. (Adapted from Bendriem and Townsend 1998)

radially inward from the detector elements (Fig. 1.15a–c). The Advance PET scanner (General Electric Medical Systems), for example, employs tungsten septa 1 mm thick and 12 cm long. In this approach, known as two-dimensional (2D) PET, these inter-ring annular septa define plane-by-plane LORs and largely eliminate out-of-plane annihilation γ -rays. By eliminating most of the contribution from out-of-plane randoms and scatter, image quality is improved, especially for large-volume sources (i.e., as in whole-body PET). However, 2D PET also eliminates most of the trues and thus considerably reduces sensitivity. Typically, both “direct” and “cross” image planes are reconstructed from LORs within the same detector ring [corresponding to a so-called “ring difference (Δ)” of 0] and between two adjacent detector rings (ring difference of ± 1), respectively. In the EXACT HR+ 2D (Siemens-CTI) PET scanner, for example, 32 detector rings span an axial FOV of 15.5 cm, yielding a total of 63 contiguous image planes comprising 32 direct and 31 cross planes. The cross-planes lie halfway between the direct planes defined by the detector elements and, conceptually, can be assigned to a “virtual” ring of detectors lying midway between two adjacent detector rings. Because the cross-plane images result from two LORs and the direct-plane images from only one, the cross-plane image sensitivity is about twice that of the direct-plane images (Fig. 1.15a–c). In an uncorrected PET study of a uniform volume source, this

results in alternating lower-count and higher-count transverse section images. In the newer 2D PET systems, LORs among as many as three adjacent rings, corresponding to a ring difference of ± 2 , are used to improve sensitivity. Increasing the ring difference does, however, degrade spatial resolution somewhat. Removing the septa altogether and including coincidence events from all of the LORs among all the detectors significantly increases PET detector sensitivity (Fig. 1.15d) – a system with $\sim 10,000$ detector elements has approximately 100 million LORs. This is known as three-dimensional (3D) PET, and is widely used among state-of-the-art PET scanners. Sensitivity is increased approximately fivefold in 3D relative to 2D PET – but with a considerable increase in the randoms and scatter count rates. Clinically, the scatter-to-true count rate ratios range from 0.2 (2D) to 0.5 (3D) in brain and from 0.4 (2D) to 2 (3D) in the whole body. To compensate for the increase in scatter count rates, new detector materials (such as GSO and LSO) were developed with better energy resolution (permitting a narrower energy window for improved scatter rejection) and accurate scatter-correction algorithms were developed for 3D PET. These detectors also respond much faster to an absorbed event allowing shorter coincidence timing windows to minimize the increased randoms count rates and dead-time count-rate losses. Data processing time for 3D PET is about an order of magnitude longer than for 2D PET. Axial sensitivity is also affected by removing the inter-ring septa: in contrast to the relatively uniform axial sensitivity for 2D PET, the axial sensitivity profile for a 3D PET scanner is triangular and peaks at the center of the FOV (Fig. 1.15d). To yield uniform sensitivity for whole-body images whole-body 3D PET studies require considerable overlap of adjacent bed-position acquisitions – optimally, one-half of the axial FOVs. In PET in general and 3D PET in particular, due to the lack of lead septa, it is important that the ends of the detector assembly are adequately shielded to minimize the contribution of counts from activity outside the axial FOV. This can be important since about 30% of the injected activity may be in the brain.

To date, only four detector materials – all inorganic scintillators – have been widely used in PET scanners: thallium-doped sodium iodide [NaI(Tl), NaI:Tl], bismuth germanate (BGO, $\text{Bi}_4\text{Ge}_3\text{O}_{12}$), cerium-doped lutetium oxyorthosilicate (LSO(Ce) or simply LSO, $\text{Lu}_2\text{SiO}_5\text{:Ce}$), and cerium-doped gadolinium oxyorthosilicate (GSO(Ce) or simply GSO, $\text{Gd}_2\text{SiO}_5\text{:Ce}$). The most important practical features of scintillation detectors include: high mass density (ρ) and effective atomic number (Z_{eff}) – to maximize the photon stopping power (i.e., intrinsic efficiency) of the detector; high light (scintillation) output – to maximize the signal and thus minimize statistical uncertainty in the energy of the detected signal; and speed of the output light pulse –

permit minimizing the coincidence timing window (τ) and random events, without sacrificing a significant portion of the signal. Higher- ρ and $-Z_{\text{eff}}$ atomic materials, such as BGO, LSO, and GSO, have emerged as the detectors of choice for PET because of their greater stopping power for 511-keV annihilation γ -rays. The MFP for 511-keV γ -rays is at least twice as long in NaI(Tl) as in BGO, GSO, or LSO. Among the latter three materials, GSO and LSO have a faster light output – nearly tenfold faster – than BGO, with LSO having a much greater light output – approximately threefold greater than either BGO or GSO. GSO has somewhat better energy resolution, and scatter rejection capability, than either BGO or LSO. A notable disadvantage of LSO is the presence of a naturally occurring long-lived radioisotope of lutetium, lutetium-177. Lutetium-177 has an isotopic abundance of 2.6% and a half-life of $\sim 4 \times 10^{10}$ years and emits two prompt γ -rays (88% abundance) of 201 and 306 keV in energy; the summed energy of 507 keV falls well within the 511-keV energy windows commonly used in PET scanners. The presence of lutetium-177 results in a measured background count rate of 240 cps/cm³ of LSO and singles and trues count rates of 100,000 and 10,000 cps, respectively, for clinical LSO PET scanners. Although the former has a negligible effect on typical emission scan, the latter would significantly increase the statistical uncertainty (noise) in single-photon transmission scans (e.g., with cesium-137) used for attenuation correction.

For 2D scanners, the so-called noise-equivalent count rate (NECR), a widely used practical measure of PET scanner sensitivity, increases linearly with activity and there is no optimal count rate or activity. For 3D scanners, on the other hand, the trues and scatter count rates are proportional to the activity while the randoms count rate is proportional to the square of the activity. Thus, there exists a well-defined optimum activity in the FOV for 3D scanners above which the random count rate begins to significantly affect image quality. The faster the detectors, and therefore the shorter the coincidence window τ can be made, the lower the randoms count rate for a given activity. Consequently, the NECR occurs at a higher administered activity and its maximum value is increased. A “fast” 3D LSO scanner ($\tau \approx 6$ ns) has a maximum NECR severalfold higher than that of a “slower” 3D BGO scanner ($\tau \approx 12$ ns). A fast 3D scanner allows the use of higher administered activities and yields high “usable” count rates, short scan durations, and increased patient throughput. At clinical activities [e.g., 185–370 MBq (5–10 mCi) of fluorine-18], however, even “slow” 3D scanners have substantially higher sensitivities and NECRs than 2D scanners.

1.4.4.4

Data Processing and Tomographic Image Reconstruction

Normalization. Even optimally performing SPECT or PET scanners exhibit some non-uniformity of response. Among the thousands of pixels in a SPECT projection image and the thousands of detector elements (and therefore LORs) in a PET scanner, slight variations in detector thickness, light emission properties, electronics performance, etc., result in slightly different measured count rates for the same activity. In principle, such non-uniform response can be corrected by acquiring data from a uniform flux of X- or γ -rays and normalizing to the *mean* count rate from all the pixels in SPECT or LORs in PET. This “normalization” table or “uniformity map” corrects for the nonuniform count rate of the individual pixels or LORs to thereby yield a pixel-by-pixel or LOR-by-LOR uniformity correction. For planar gamma camera imaging as well as SPECT, such a correction table may be acquired using either a uniform flood source placed on the detector or a point source placed sufficiently far (typically ~ 2 m) from the uncollimated detector to approximate a uniform photon flux (see below). For PET, it may be acquired using a positron-emitting rod source (e.g., germanium-68) spanning the entire axial FOV and rotating it around the periphery of the FOV, exposing the detector pairs to a uniform photon flux per revolution. Alternatively, a uniform cylinder of a positron-emitting radionuclide can be scanned and the data thus acquired analytically corrected for attenuation; for a well-defined geometry such as a uniform cylindrical source, this correction is straightforward. However, for 3D PET, the contribution of, and correction for, scatter with such a large-volume source are non-trivial. For both planar imaging as well as SPECT and PET, acquisition of the data required for uniformity correction is somewhat problematic in practice because of statistical considerations: tens of millions (SPECT) to hundreds of millions (PET) of counts must be acquired to avoid possible “noise”-related artifacts in the uniformity correction table.

Deadtime Correction. Scintillation detectors have a finite deadtime and associated count losses. The deadtime is the length of time required for a counting system to record an event, during which additional events cannot be recorded. As a result, the measured count rate is lower than the actual count rate. Such count losses are significant, however, only at “high” count rates and are generally minimal at clinical administered activities. Nonetheless, a real-time correction for deadtime count losses is routinely applied in PET (though not in SPECT) to the measured count rates, most commonly by scaling up the measured count rate based on an empirically derived mathematical relationship between measured and true count rates.

Center-of-Rotation Misalignment Correction (SPECT). In rotating-gamma camera SPECT, the location of the projection of the center of rotation (COR) on the projection image matrix must be constant. If the mechanical and electronic CORs are aligned, the pixel location of the projection of the COR onto the projection image matrix will be the same for all projection images and, for all such images, the counts in each pixel will then be projected across the appropriate row of pixels in the tomographic image matrix. If, however, the mechanical and electronic CORs are not aligned, the pixel location of the COR will vary among the projection images and the counts in each projection-image pixel will be projected across different locations in the tomographic image matrix and blurred images will result (Fig. 1.16a). In today’s SPECT systems, COR misalignment may be easily measured and corrections created and automatically applied using the system’s software (Fig. 1.16b).

Randoms Correction (PET). In PET, randoms increase the detected coincidence count rate by introducing mis-positioned events and thus reduce image contrast and distort the relationship between image intensity and activity concentration. The standard approach to randoms correction, the “delayed window” method, is based on the fact that the random-coincidence γ -rays are temporally uncorrelated (i.e., not simultaneously emitted). Briefly, once singles in the coincidence timing window (typically 6 – 12 ns) are detected, the number of singles in a timing window equal in duration to, but much later (> 50 ns later) than, the coincidence timing window are determined. The number of events in the delayed timing window provides an estimate of the number of randoms in the coincidence timing window. Real-time subtraction of the delayed-window counts from the coincidence-window counts for each LOR thus corrects for randoms.

Scatter Correction. Scatter results in generally diffuse background counts in reconstructed images, reducing contrast and distorting the relationship between image intensity and activity concentration. In PET in general and 2D PET in particular, scatter correction is rather straightforward. Once the randoms correction has been applied, the peripheral “tails” in the projection-image count profiles, presumably due exclusively to scatter, are fitted to a mathematical function and then subtracted (deconvolved) from the measured profile to yield scatter-corrected profiles for tomographic image reconstruction. While this approach works reasonably well for 2D PET and small source volumes (e.g., the brain) in 3D PET, it is generally not adequate for 3D PET. Scatter corrections for 3D PET include: dual energy window-based approaches; convolution/deconvolution-based approaches (analogous to

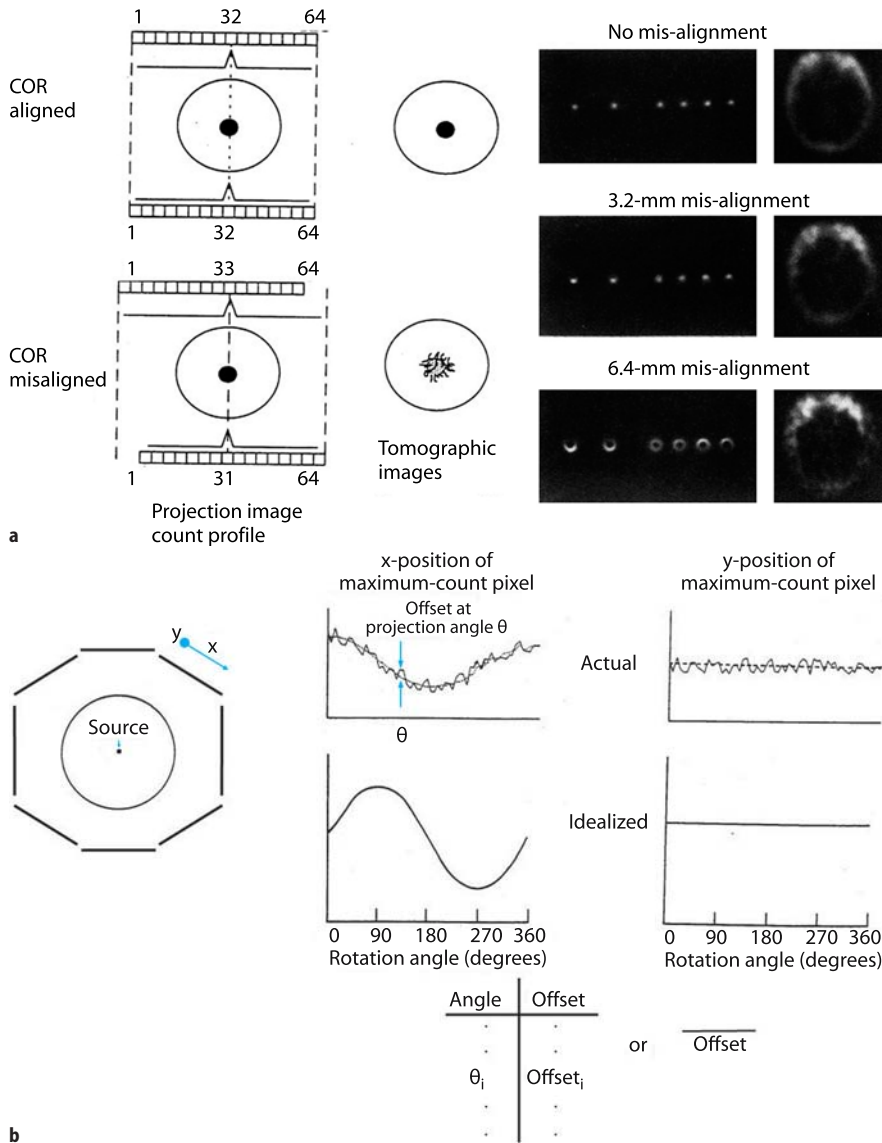


Fig. 1.16. **a** Center-of-rotation (COR) misalignment and resulting image-blurring artifacts in rotating-gamma camera SPECT. The degree of blurring is related to the magnitude of the spatial misalignment of the mechanical and electronic CORs. A misalignment as small as 3.2 mm (or 1/2 a pixel for a 64×64-image matrix) can produce perceptible blurring in SPECT images, with the blurring substantially worse for a misalignment of 6.4 mm (1 pixel). **b** COR misalignment can be measured and corrected based on acquiring a 360° circular SPECT study of a ^{99m}Tc point source and constructing graphs of the x - and y -positions (perpendicular and parallel to the axis of rotation, respectively) of the position of the maximum-count pixel in each projection image versus angular position. The x - and y -position-versus-angle graphs should be a sinusoidal curve and a straight line, respectively. The angle-by-angle deviation between the x -position on the best-fit sine curve and the x -position of the actual maximum-count pixel thus yields a correction table indicating the offset by which each projection image must be shifted at each angular position to align the CORs. Alternatively, the average of the offsets may be used at each angular position. (Adapted from Zanzonico 1995 in the “Further Reading” list)

the correction in 2D PET); direct estimation of scatter distribution (by Monte Carlo simulation of the imaging system); and iterative reconstruction-based scatter compensation approaches (also employing Monte Carlo simulation). The Monte Carlo simulation and subtraction of scatter have been implemented in commercial PET scanners.

Scatter corrections in SPECT are not yet as well developed or as reliable. Perhaps the most widely used approach is the “dual-window” method in which a “scatter” energy window [equal in width (in keV) to the photopeak energy window] is created and two separate images, a scatter and a photopeak image, simultaneously acquired. The scatter image is then multiplied by a fractional weighting factor, to estimate the pixel-by-pixel scatter counts appearing in the photopeak im-

age, and the weighted scatter image is then subtracted from the photopeak image.

Attenuation Correction. Attenuation correction is generally the largest correction in tomographic imaging. In contrast to SPECT, one of the most attractive features of PET is the relative ease of applying accurate and precise corrections for attenuation, based on the fact that attenuation depends only on the total thickness of the attenuation medium. For a positron-emitting source and a volume of thickness L , the attenuation factor is $e^{-\mu L}$ and the attenuation correction factor $e^{\mu L}$ regardless of the position of the source. Accordingly, if a rod source of a positron emitter such as germanium-68 is extended along the axial FOV and rotated around the periphery of the FOV first with and then without

the patient in the imaging position – the transmission and the blank scans, respectively – the attenuation correction factor (ACF) can be derived from the ratio of the counts in these respective scans:

$$ACF_{ij} = e^{\mu L_{ij}} \quad (1.18)$$

$$ACF_{ij} = \frac{[(C)_{\text{Blank}}]_{ij}}{[(C)_{\text{Trans}}]_{ij}} \quad (1.19)$$

where ACF_{ij} = the attenuation correction factor between coincident detectors i and j , L_{ij} = the thickness of the volume between coincident detectors i and j , and $[(C)_{\text{Blank}}]_{ij}$ and $[(C)_{\text{Trans}}]_{ij}$ = the external-source counts between detectors i and j in the blank and transmission scans, respectively. In practice, a blank scan is acquired only once a day. The transmission scan can be acquired before the patient has been injected with the radiopharmaceutical, after the patient has been injected with the radiopharmaceutical but before or after the emission scan, or after the patient has been injected with the radiopharmaceutical and at the same time as the emission scan. Pre-injection transmission scanning avoids any interferences between the emission and transmission data but requires that the patient remain on the imaging table before, during, and after injection of the radiotracer. It is the least efficient operationally and is rarely used in practice. Post-injection transmission scanning minimizes the effects of patient motion, relying on the much higher external-source count rates for reliable subtraction of the emission counts from the transmission counts. It is probably the most commonly used approach in “PET-only” scanners. Simultaneous emission/transmission scanning is obviously the most efficient (fastest) approach but may result in excessively high randoms and scatter counter rates in the emission data. The GE Advance employs post-injection transmission scanning using two germanium-68 rod sources each with 370 MBq (10 mCi) and a 4- to 6-min transmission scan per bed position. With the recent introduction of PET-CT scanners, attenuation correction may now be performed using CT rather than transmission sources. A CT image is basically a two-dimensional map of attenuation coefficients at the CT X-ray energy (~80 keV). For attenuation correction of the PET emission data, however, these must be appropriately scaled to the 511-keV energy of the annihilation γ -rays. The mass-attenuation coefficients (μ_m) for CT X-rays (~80 keV) and for 511-keV annihilation γ -rays are 0.182 and 0.096 cm²/g, 0.209 and 0.093 cm²/g, and 0.167 and 0.087 cm²/g in soft tissue, bone, and lung, respectively. The corresponding μ_m ratios are therefore 1.90, 2.26, and 1.92, respectively. Thus, ACFs derived from CT images cannot be scaled to those for 511-keV annihilation γ -rays simply using a global factor. Accordingly, CT-based attenuation correction in PET has been implemented using a combination of segmentation – to

delineate soft tissue, bone, and lung compartments – and variable scaling – to account for the different μ_m ratios in these respective tissues.

Like scatter corrections, attenuation corrections in SPECT are not yet as well developed or as reliable as those in PET. For many years, if attempted at all, SPECT attenuation correction factors were calculated (as in Chang’s first-order correction and the Sorenson method) based on the assumptions – neither of which is generally true – that the body is a uniform medium with a single, well-defined value of μ and that the body’s contour is known. More recently, manufacturers have incorporated long-lived radioactive sources (such as gadolinium-153) into SPECT scanners to perform attenuation correction. As part of the SPECT procedure, a shutter opens at each projection-image angle and exposes a highly collimated line source and a transmission image is acquired. The transmission images thus acquired are reconstructed into an ACF map for correction of the SPECT study. The recent introduction of SPECT-CT scanners will likely result in more practical and more accurate attenuation correction in SPECT.

Image Reconstruction. In SPECT and in 2D PET, the emission data are the one-dimensional projections [sets of parallel line-integrals (ray sums)] of the direct planes at the azimuthal, or projection, angles θ relative to the axis of the scanner. The full set of 2D projection data are usually represented as a two-dimensional matrix in polar coordinates (distance x , angle ϕ) known as a “sinogram” (or “histogram”) in which each row represents the projected intensity across a single direct plane and each column the projected intensity at the same distance x , across the projection at successive azimuthal angles θ (Fig. 1.17a). In 3D PET, the projections are two-dimensional (x , y) *parallel line-integrals with azimuthal angle ϕ and oblique, or polar, angle θ* . The full set of 3D projection data are then represented as a set of sinograms, with one sinogram per polar angle ϕ . In each sinogram, each row represents the projected intensity across a single oblique plane (at polar angle θ) and each column the projected intensity at the same position across the projection at successive azimuthal angles ϕ (Fig. 1.17b).

Analytic methods for reconstruction of 3D data characteristically suffer from incomplete sampling of the 3D volume as a result of the finite axial FOV of PET scanners. The three-dimensional re-projection (3DRP) algorithm, an extension of the standard 2D FBP algorithm (see below), has been the most widely used 3D reconstruction algorithm and has been implemented on commercial 3D scanners. In 3DRP, unsampled data are estimated by reconstruction and then 3D forward-projection of an initial image set obtained by reconstruction of the directly measured data. Such 3D reconstruction algorithms remain computer-intensive and

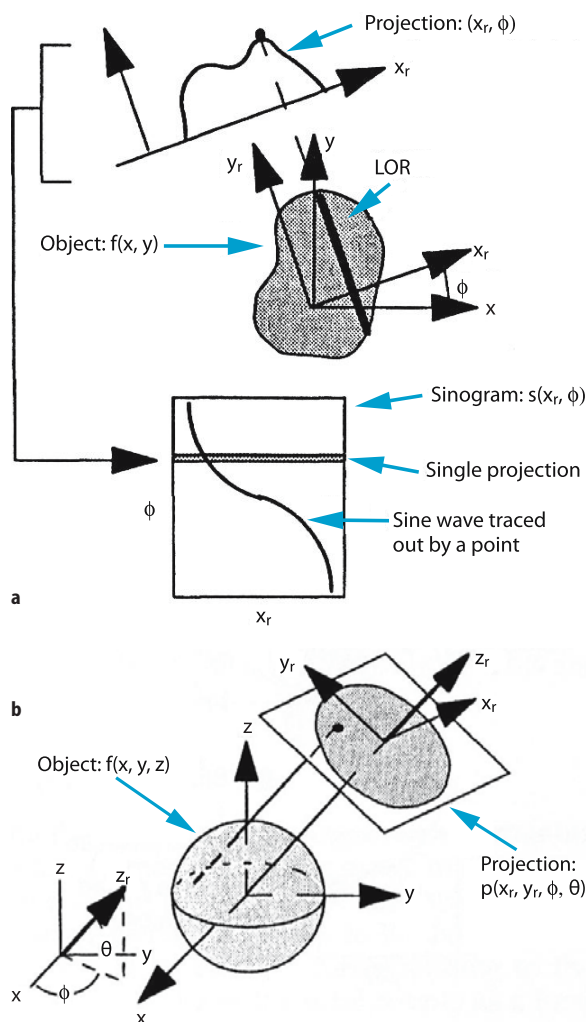


Fig. 1.17. **a** In 2D PET, the emission data are the one-dimensional projections (sets of parallel line-integrals) of the direct planes at the azimuthal angles ϕ relative to the axis of the scanner. In the sinogram, each row represents the projected intensity across a single direct plane and each column the projected intensity at the same distance x_r across the projection at successive azimuthal angles ϕ . **b** In 3D PET, the projections are two-dimensional (x_r, y_r) parallel line-integrals with azimuthal angle ϕ and oblique angle θ . The 3D projection data are represented as a set of sinograms, with one sinogram per polar angle θ , each row representing the projected intensity across a single polar angle θ and each column the projected intensity at the same position x_r across the projection at successive azimuthal angles ϕ . (Adapted from Bendriem and Townsend 1998)

rather slow by clinical standards, however. In addition, 3D PET emission data files are very large – typically more than two orders of magnitude larger than 2D data sets. It is preferable, therefore, to reduce 3D data sets to a more manageable size for image reconstruction – by re-binning of the 3D set of oblique sinograms into a smaller number of direct 2D sinograms. The simplest method is “single-slice re-binning (SSRB),” wherein

true oblique LORs are assigned to the direct plane midway between the two detector elements actually in coincidence. SSRB distorts off-axis activity and thus is accurate only for activity distributions close to the detector axis, as in brain or small-animal imaging. A second method is multi-slice re-binning (MSRB), which is fast but is susceptible to “noise”-related artifacts. The current method of choice is Fourier re-binning (FORE), based on the 2D Fourier transform of the oblique sinograms. In contrast to SSRB and MSRB, however, FORE cannot be performed in real-time and thus requires the full 3D data set.

After 2D re-binning of 3D data, 2D reconstruction algorithms can be used for 3D PET as well as 2D PET and SPECT data. Note that processing of the emission data after the real-time deadtime and randoms corrections and before image reconstruction – namely, normalization, scatter correction, and then attenuation correction – is normally performed in sinogram space. One of the most widely used algorithms for reconstruction of tomographic images from 2D data (or 3D data re-binned into 2D projections) – in SPECT as well as PET – remains filtered back-projection (FBP). The basic procedure is as follows: each projection is Fourier transformed from real to frequency space; the projection is filtered in frequency space using a ramp filter; the filtered projection is inverse Fourier transformed from frequency back to real space; and the filtered projection data in real space are uniformly distributed, or back-projected, over the reconstructed image matrix. The resulting reconstructed image is inexact, however, because the ramp filter results in the inclusion of spatial frequencies beyond the maximum frequency imageable by the scanner (i.e., the Nyquist frequency, ν_N) – producing aliasing artifacts (such as the “starburst” pattern emanating from discrete, high-activity foci) – and amplifies statistical uncertainty (noise or mottle). To compensate for these effects, low-pass, or apodizing, filters (known as Hanning, Butterworth, etc.) are used in place of the ramp filter to eliminate those spatial frequencies above a cut-off frequency, ν_c , set equal to ν_N or some fraction thereof. Although the resulting reconstructed images have somewhat degraded spatial resolution, they are far less “noisy” (mottled).

In contrast to so-called “transform” reconstruction methods such as FBP, iterative algorithms attempt to progressively refine estimates of the activity distribution, rather than directly calculating the distribution, by maximizing or minimizing some “target function.” The solution is said to “converge” when the difference of the target function between successive estimates (iterations) of the activity distribution is less than some pre-specified value. Importantly, iterative reconstruction algorithms allow incorporation of realistic modeling of the data acquisition process (including effects of attenuation and of scatter), modeling of statistical

noise, and inclusion of pertinent a priori information (e.g., only non-negative count values). The maximum-likelihood expectation maximization (MLEM) algorithm is based on maximizing the logarithm of a Poisson-likelihood target function. The MLEM algorithm suppresses statistical noise, but large numbers of iterations typically are required for convergence and therefore processing times are long. To accelerate this slow convergence, the ordered-subset expectation maximization (OSEM) algorithm groups the projection data into subsets composed of projections uniformly distributed around the source volume. The OSEM algorithm, which is a modified version of the MLEM algorithm in that the target is still a maximization of the log-likelihood function, converges more rapidly than MLEM and is now the most widely used iterative reconstruction method in PET as well as SPECT. The row-action maximization-likelihood (RAMLA) algorithm, related to the OSEM algorithm, has been implemented for direct reconstruction of 3D PET data in the C-PET and Allegro (Philips ADAC). The so-called 3D-RAMLA algorithm, which eliminates 2D re-binning of the 3D data, employs partially overlapping, spherically symmetric volume elements called “blobs” in place of voxels. Reconstruction times are fairly long by clinical standards but the results have been excellent.

Quantitation. Once the PET emission data have been corrected for deadtime, randoms, system response (by normalization), scatter, and attenuation, the count rate per voxel in the reconstructed tomographic images is proportional to the local activity concentration. [In principle, SPECT images can be made quantitative in an analogous manner. In practice, however, the pertinent corrections (especially scatter and attenuation corrections) are not as reliable in SPECT as in PET, as previously noted.] To make the images quantitative, then, the count rate per voxel (cps), \dot{C}_{ijk} , in voxel ijk should be divided by the measured system calibration factor $[(\mu\text{Ci/cc})/(\text{cps/voxel})]$, CF, to yield the activity concentration:

$$[A]_{ijk} = \frac{\dot{C}_{ijk}}{\text{CF}} \quad (1.20)$$

where $[A]_{ijk}$ = the activity concentration ($\mu\text{Ci/cc}$) in voxel ijk . The calibration factor CF can be derived by scanning a calibrated standard, that is, a water-filled or water (tissue)-equivalent volume source with all linear dimensions at least twice that of the system spatial resolution (FWHM) and with a uniform, well-defined activity concentration at the time of the scan. The requirement for water equivalence is to ensure that effects such as scatter and attenuation are comparable in both the patient and the standard. And the requirement for linear dimensions at least twice that of the system spatial resolution is to ensure that the effects of partial

volume averaging and associated underestimation of local count rates are negligible. Typically, a more clinically relevant expression of local activity concentration is in terms of the decay-corrected fraction or percent of the administered activity per cubic centimeter (cc) or, more commonly, in terms of the standard uptake value (SUV):

$$\text{SUV} \equiv \frac{\mu\text{Ci/cc of tissue}}{\mu\text{Ci injected/gm body mass}} \quad (1.21)$$

1.4.5

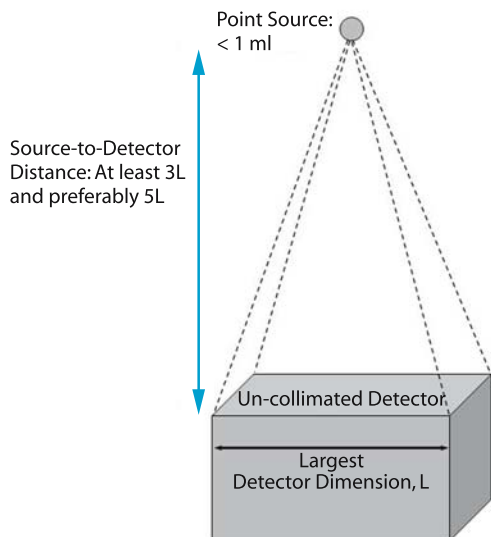
Gamma Camera Performance and Quality Control

Quality control (QC), a critical component of analytical procedures and instrumentation in general and medical devices in particular, is an established set of ongoing measurements and analyses designed to ensure that the performance of a procedure or instrument is within a pre-defined acceptable range. An extensive series of parameters have been developed over the years to characterize gamma camera, SPECT scanner, and PET scanner performance, and detailed data acquisition and analysis protocols have been promulgated by the National Electrical Manufacturers Association (NEMA), the American Association of Physicists in Medicine (AAPM), and others for this purpose. In practice, however, less extensive and less rigorous procedures have proven adequate for day-to-day QC.

To understand gamma camera performance and routine QC, several pertinent terms – intrinsic versus extrinsic (or system) performance and the useful versus the central field of view – must be understood. Intrinsic performance refers to gamma camera performance without a collimator in place while extrinsic (or system) performance refers to that of the entire gamma system, including collimation. The useful field of view (UFOV) of a gamma camera is essentially the entire detector (i.e., crystal) area while the central field of view (CFOV) corresponds to the inner, or central, 3/4 of the crystal area. The periphery of the gamma camera detector suffers from artifacts (e.g., edge packing) and poorer image quality in general, in part because light reflected from the mirror-like inner surface of the detector housing makes it appear that a disproportionate amount of light is emanating from this peripheral area. Accordingly, the periphery of the crystal is masked (or shielded), often by lead built into the edges of the collimator housing. Thus, the CFOV is the portion of the detector actually used in clinical imaging.

The performance parameters most commonly evaluated as part of a routine gamma camera QC program include uniformity, spatial resolution, and energy resolution (see above). Uniformity (the so-called “daily flood”) should be evaluated each day either intrinsically or extrinsically (Fig. 1.18). Either $^{99\text{m}}\text{Tc}$ (intrinsic) or

Intrinsic uniformity



Extrinsic uniformity

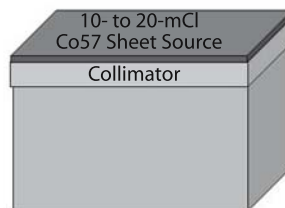


Fig. 1.18. Gamma camera uniformity may be evaluated either intrinsically or extrinsically. Intrinsically, a “point” source (<math>< 1\text{ ml}</math> in volume and containing $\sim 500\text{ mCi}$) of $^{99\text{m}}\text{Tc}$ (at least for daily evaluation of uniformity) is placed at least three and preferably five crystal dimensions from and centered over the uncollimated detector to approximate a uniform photon flux. If necessary, the activity should be adjusted to yield a measured count rate no greater than 25,000 cps (to avoid deadtime counting losses and count rate-related image degradation). Extrinsically, a uniform flood, or sheet, source (typically 10–20 mCi) of ^{57}Co (for daily evaluation of uniformity) is

placed directly on the collimated detector. ^{57}Co , known as “mock $^{99\text{m}}\text{Tc}$,” has a half-life of 270 days and emits a 122-keV γ -ray and is thus a convenient, long-lived alternative to $^{99\text{m}}\text{Tc}$. Such ^{57}Co sheet sources are available commercially. A total of 10–15 million counts should be acquired and uniformity evaluated quantitatively (e.g., in terms of the integral and differential uniformities; Eq. 1.17)

^{57}Co (extrinsic) is used on a daily basis. Periodically (e.g., monthly), however, intrinsic uniformity for other radionuclides used clinically (e.g., ^{67}Ga , ^{111}In , and ^{131}I) should also be evaluated. Integral uniformities (Eq. 1.17), or IUs, up to 5% are acceptable, although nowadays IUs of 3% or better are routinely obtained. If the uniformity for any radionuclide is out of tolerance (i.e., > 5%), that radionuclide’s uniformity (or sensitivity) correction table should be updated. The necessary data may be acquired using the same set-up as for the daily uniformity test, except that a much larger number of counts (60–100 million) must be acquired. In today’s gamma cameras, uniformity correction tables may be easily updated and the corrections created, processed, stored, and automatically applied using the system’s integrated software. In addition to an outdated uniformity correction table, there are other causes of gamma camera uniformity (Fig. 1.19 and 1.20): mis-tuning (detuning), un-coupling of a PMT; a cracked crystal; or corruption or switching off of one or more of the camera’s correction tables (i.e., its energy, uniformity, and/or linearity correction tables).

Spatial resolution, in practice, is generally assessed using some sort of resolution phantom (or mask), the four-quadrant bar-phantom perhaps being the one most widely used (Fig. 1.21). This should be done at least weekly. Gamma camera energy resolution per se is not generally evaluated on a routine basis. However, the energy spectrum for each radionuclide used clinically should be checked at least once a day to verify that the photopeak(s) is (are) centered in the photopeak energy

window(s) currently set (Fig. 1.6b). Ideally, the energy spectrum should be checked for each patient.

In addition to the foregoing QC procedures for gamma camera imaging generally, rotating-gamma camera SPECT requires QC as well. Among the components of a routine SPECT QC program are periodic assessment of COR alignment (Fig. 1.16), tomographic uniformity, and, for lack of a better term, overall system performance. As described above and in Fig. 1.16, proper alignment of the mechanical and electronic CORs is critical in rotating-gamma camera SPECT and should be checked and, if necessary, the COR misalignment correction updated at least weekly. Tomographic uniformity may be evaluated by imaging a uniform cylinder source (at least 20 cm in diameter) and visually inspecting the resulting images for the absence of rings, or “bulls eye,” attributable to system non-uniformity. Overall system performance may be evaluated using any number of commercially available fillable phantoms containing non-radioactive (“cold”) inserts of different sizes and visually inspecting the resulting images to determine the size of the smallest insert that is visible. Typically, such a phantom will include a uniform portion that is used to simultaneously evaluate tomographic uniformity. PET tomographic uniformity and overall system performance may also be evaluated using such phantoms.

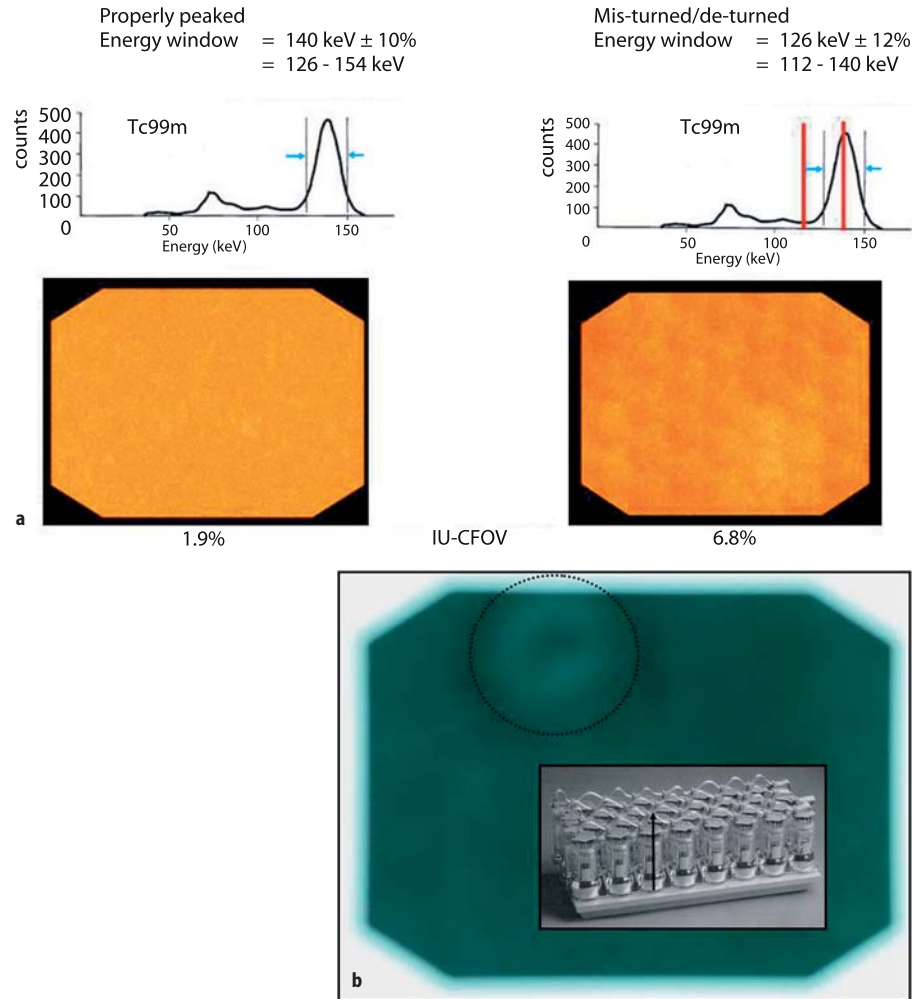
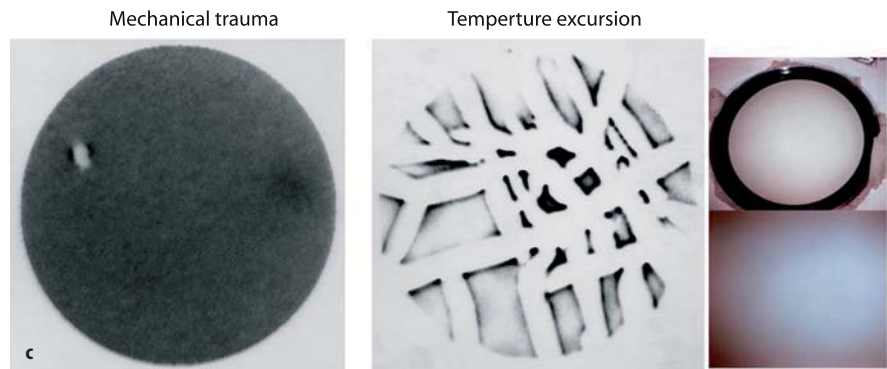


Fig. 1.19. Sources of gamma camera non-uniformity.

a Mis-tuning (or de-tuning), meaning that the radionuclide's photopeak does not coincide with the camera's photopeak energy window, perhaps because the photopeak energy window (as shown) and/or the PMTs' high voltages are not set correctly. **b** Un-coupling of a PMT from the crystal, resulting in loss of all or part of the light signal in the resulting air gap between the PMT entrance window and the crystal. **c** Cracked crystal, either due to mechanical trauma (an impact) or a temperature excursion (i.e., a temperature increase or decrease at a rate faster than $\sim 5^\circ\text{C}$ per hour causing the crystal to expand or contract, respectively, to the point of cracking). Note that it is the *rate* of the temperature change which is critical. The photographs *on the right* show the cracked crystal which produced the "temperature-excursion" image. Even though the cracks are grossly imperceptible, the artifacts produced are very dramatic. **d** Corrupted, deleted, or switched-off software correction tables. Even perfectly functioning gamma cameras have some non-uniformity due to ill-defined factors such as variations in crystal thickness. The associated non-uniformities are measured and used to create energy, linearity, and uniformity (or sensitivity) correction tables, respectively. Note that the linearity correction table has the biggest impact on uniformity: if corrupted, deleted, or switched-off, the PMT pattern becomes grossly apparent and the IU approaches 20%. Fortunately, in contrast to the uniformity correction table and, to a lesser extent, the energy correction table, the linearity correction table rarely needs to be updated once a gamma camera is installed; if it becomes necessary, it is almost always done by field service personnel, not the end-user



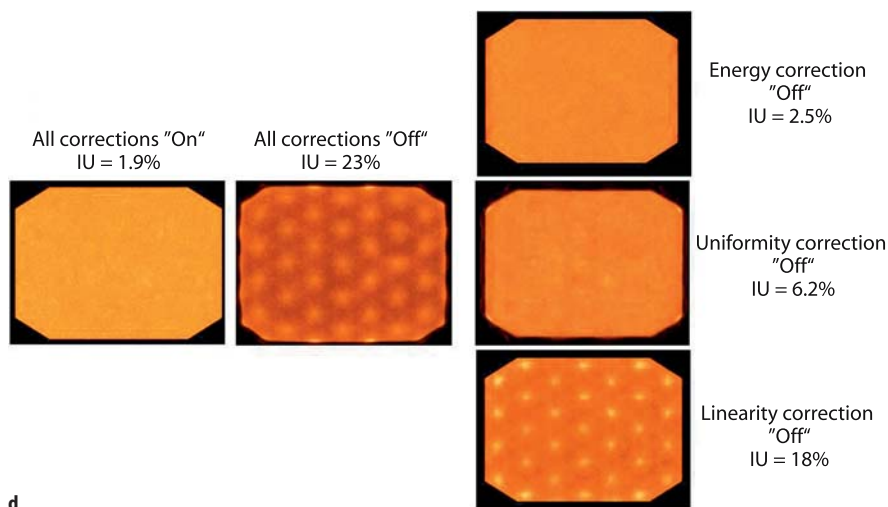


Fig. 1.19.(Cont.)

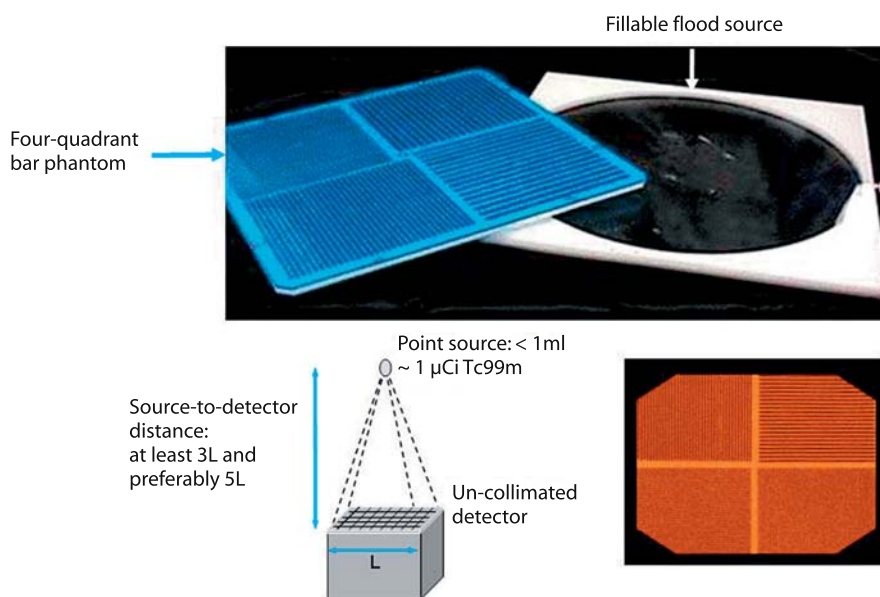


Fig. 1.20. In practice, intrinsic gamma camera resolution is often evaluated using a four-quadrant bar phantom, consisting of radiopaque lead bars and intervening radiolucent plastic strips 2, 2.5, 3, and 4 mm in width. A “point” source (<math>< 1 \text{ ml}</math> in volume and containing $\sim 1 \mu\text{Ci}</math> of $^{99\text{m}}\text{Tc}</math> is placed at least three and preferably five crystal dimensions from and centered over the uncollimated detector, with the phantom placed directly over the detector. A 5- to 10-million-count “transmission” image is then acquired and visually inspected. The lead bars in at least the two coarsest quadrants (i.e., with the 3- and 4-mm-wide bars) should be$$


visually resolvable. [A fillable sheet source, which may be filled with different radionuclides and used to evaluate extrinsic uniformity (see Fig. 1.19) is also shown in the photograph]

1.4.6 Multi-modality Devices and Other Developments

The major manufacturers of nuclear medicine instrumentation now market multi-modality scanners, combining high-performance state-of-the-art PET and CT scanners and, more recently, SPECT and CT scanners in a single device. These instruments provide near-perfect registration of images of in vivo function (PET or SPECT) and anatomy (CT). PET-CT scanners are already having a major impact on clinical practice, particularly in oncology, and are currently far outselling “PET-only” systems 2 to 1. Although generally encased in a single seamless housing, the PET or SPECT and CT

gantries in such devices are separate; the respective FOVs are separated by a distance of the order of 1 m and the PET or SPECT and CT scans are performed sequentially. In one such device, the Gemini (Philips-ADAC), the PET and CT gantries are actually in separate housings with a sizable space between them; this not only provides access to patients but also may minimize anxiety among claustrophobic subjects. Moreover, in the Gemini the distance between the PET and CT gantries may be varied. With the incorporation of 16 and 64-slice spiral CT scanners, applications in cardiology as well as oncology are growing rapidly.

Time-of-flight (TOF) PET is based on the measurement of the difference between the detection times of



Color	White	Yellow	Yellow
Exposure Rate (mR/hr)			
On Surface	< 0.5	0.5 - 50	50 - 200
At 1 m	0	< 1	1 - 10
Type of shipment	Diagnostic unit doses	Therapy unit doses	Generators

Fig. 1.21. US DOT labels required for shipment of radioactive packages. The particular label required is dictated by the package's "transport index (TI)," defined as its exposure rate in mR/h measured at a distance of 1 m from the package surface: TI=0 (i.e., a measured exposure rate at 1 m equal to the background exposure rate) – "White I"; TI < 1 "Yellow II"; TI = 1 to 10 – "Yellow III"

the two positron-neutron annihilation photons arising from the decay of a positron, allowing spatial localization of the annihilation event along the LOR with a spatial resolution of ~ 100 mm assuming a coincidence time resolution (τ) of ~ 1 ns. Though a considerably coarser resolution than that of the conventional PET scanner (~ 5 mm), this approximate localization reduces the random coincidence rate and improves the signal-to-noise ratio (SNR), especially for large objects. For the TOF scanners developed in the 1980s, the SNR gain was offset by the low stopping power of the scintillation crystals [barium fluoride (BaF_2) and cesium fluoride (CsF)] used at the time and TOF PET was largely abandoned. Today, however, faster electronics and crystals such as LSO and GSO have made TOF PET feasible, and at least one manufacturer (Philips) has developed a commercial TOF scanner.

1.5 Radiation Safety

1.5.1 Regulatory Jurisdiction and Licensure

The use of radioactivity, particularly in medicine, is highly regulated, and extensive institutional as well as regulatory policies and procedures have been promulgated to ensure its safe and compliant use. In the United States, the use of radioactivity is primarily regulated by a federal agency, the Nuclear Regulatory Commission (NRC), pursuant to Title 10, Part 35 of the Code of Federal Regulations (10CFR35). As stated in 10CFR35, "This part contains the requirements and provisions for the medical use of byproduct material and for issuance of specific licenses authorizing the medical use of this material. These requirements and provisions provide for the radiation safety of workers, the general

public, patients, and human research subjects." However, in well over half of the states – the so-called "Agreement States," the NRC has agreed to delegate its regulatory authority to the state; in Agreement States, therefore, the use of radioactivity is directly regulated by a state agency rather than the NRC. In addition, the Food and Drug Administration (FDA), the United States Department of Transportation (US DOT), and other federal agencies maintain regulatory authority over certain aspects of the medical use of radioactivity. In any medical or other facility in which radioactive materials are used, the Radiation Safety Officer (RSO), in conjunction with a Radiation Committee and individual users, is charged with ensuring that all such materials are used in a manner which is safe and compliant with all applicable regulations.

Among the regulatory activities of the NRC and their Agreement-State counterparts are the licensing of physicians to possess radioactive materials for medical use and stipulation of the training-and-experience requirements for such licensure. For a diagnostic nuclear medicine practitioner, this includes 200 h of didactic training in the pertinent basic science (including radiation physics, radiobiology, and mathematics), 500 h of supervised training in practical radiation science, and 500 h of supervised training in clinical practice (including reading and interpreting studies). For licensure to also perform therapeutic nuclear medicine procedures, additional training and experience are required, including direct participation in the diagnosis and iodine-131 treatment of at least ten cases of hyperthyroidism and at least three cases of thyroid cancer. Physicians who are "board-eligible" for certification by the American Board of Nuclear Medicine (ABNM) and the American Board of Radiology (ABR) (special competency in nuclear medicine) will have satisfied these requirements.

1.5.2 Quantities and Units

Perhaps the most widely used and biologically meaningful quantity for expressing radiation dose, the absorbed dose, D , is defined as follows:

$$D \equiv \frac{d\bar{E}}{dm} \quad (1.22)$$

where $d\bar{E}$ is the mean energy imparted by ionizing radiation to a mass dm of matter. The SI unit is the gray (1 Gy = 1 J/kg) and the conventional unit the rad (1 rad = 100 erg/g); 1 Gy equals 100 rad and 1 rad equals 1 cGy (or 10 mGy).

Importantly, for the same absorbed dose, the frequency and/or severity of biological effects are generally less for sparsely ionizing (i.e., low-quality) than for densely ionizing (i.e., high-quality) radiations. Radia-

tion quality is characterized by the linear energy transfer, LET:

$$\text{LET} \equiv \frac{dE}{dl} \quad (1.23)$$

where dE is the energy lost by a charged particle (or the secondary charged particle produced by the primary radiation) in traversing a distance dl in matter. The SI unit is the J/m and the conventional unit the keV/ μ ; 1 J/m equals 6.25×10^9 keV/ μ and 1 keV/ μ equals 1.60×10^{-10} J/m. LET is of the order of 1 keV/ μ for X-, γ -, and β -rays, 10 keV/ μ for n and p, and 100 keV/ μ for α -rays.

The influence of LET on the frequency and/or severity of biological effects is quantified by the relative biological effectiveness, RBE:

$$\text{RBE}(A) \equiv \frac{D_{\text{reference}}}{D_A} \quad (1.24)$$

where $D_{\text{reference}}$ is the absorbed dose of reference radiation (typically a widely available sparsely ionizing radiation such as cobalt-60 γ -rays) required to produce a specific biological effect and D_A is the absorbed dose of radiation A required to produce the same frequency and/or severity of the same specific biological effect with all pertinent parameters maintained as identical as possible. The RBE is a ratio of absorbed doses and thus is a dimensionless quantity. While its actual value for a given radiation depends on the specific biological effect, the conditions of the irradiation, etc., RBE is typically ~ 1 for X-, γ -, and β -rays, 5–10 for n and p, and 10–20 for α -rays. A simplified version of the RBE, the radiation weighting factor, w_R , was devised for purposes of radiation protection. The equivalent dose, H_T , in tissue or organ T, is related to the radiation weighting factors, w_R , and the mean absorbed doses, $D_{T,R}$, to tissue or organ T due to radiations R:

$$H_T \equiv \sum_R w_R D_{T,R} \quad (1.25)$$

where w_R is assigned a value of 1 for X-, γ -, and β -rays, 2 for p, 5–20 for n, and 20 for α -rays. The radiation weighting factor, w_R , and the equivalent dose, H_T , are similar to the older quantities of quality factor, Q , and dose equivalent, H , respectively.

The effective dose (E) is intended to provide a single-value estimate of the overall stochastic risk (i.e., the total risk of cancer and genetic defects) of a given irradiation whether received by the whole body, part of the body, or only one or several individual organs:

$$E \equiv \sum_T w_T H_T \quad (1.26)$$

$$E \equiv \sum_T \sum_R w_T w_R D_{T,R} \quad (1.27)$$

where w_T is the weighting factor for tissue or organ T, a dimensionless quantity representing the fraction con-

tributed by tissue or organ T to the *total* stochastic risk (i.e., $w_T = 0.01$ for bone and skin; 0.05 for bladder, breast, esophagus, liver, thyroid, and remainder of body; 0.12 for bone marrow, colon, lung, and stomach; and 0.20 for gonads). The effective dose is similar in concept to the effective dose equivalent, H_E (introduced previously by the ICRP and the NCRP), representing a single-value estimate of the net “harm” from any “low-dose” (e.g., diagnostic nuclear medicine or occupational) exposure. The effective dose and the effective dose equivalent do not apply to, and should not be used for, “high-dose” (e.g., therapeutic nuclear medicine) exposures. For both equivalent dose and the effective dose, the SI unit is the sievert (1 Sv = 1 J/kg) and the conventional unit the rem (1 rem = 100 erg/g); 1 Sv equals 100 rem and 1 rem equals 1 cSv (or 10 mSv).

1.5.3

Sources of Radiation Exposure and Dose Limits

Human beings are constantly and universally exposed to background radiation – from cosmic radiation from outer space, naturally occurring radionuclides in our environment and our own bodies, and other sources (Table 1.4). In the United States, the total exposure (actually, effective dose equivalent) averages 3.6 mSv, or

Table 1.4. Average annual radiation dose (expressed as dose equivalent and effective dose equivalent) to the US population, 1987. (Source: National Council on Radiation Protection and Measurements)

Source	Dose equivalent ^a		Effective dose equivalent	
	mSv	mrem	mSv	%
Natural				
Natural radon ^b	24	2,400	2.0	55
Cosmic	0.27	27	0.27	8.0
Terrestrial	0.28	28	0.28	8.0
Internal	0.39	39	0.39	11
Total natural	–	–	3.0	82
Artificial				
Medical				
X-ray diagnosis	0.39	39	0.39	11
Nuclear medicine	0.14	14	0.14	4.0
Consumer products	0.10	10	0.10	3.0
Other				
Occupational	0.009	0.9	<0.01	<0.3
Nuclear fuel cycle	<0.01	<1.0	<0.01	<0.03
Fallout	<0.01	<1.0	<0.01	<0.03
Miscellaneous ^c	<0.01	<1.0	<0.01	<0.03
Total artificial	–	–	0.63	18
Total natural and artificial	–	–	3.6	100

^a To soft tissues

^b Dose equivalent to bronchi from radon daughter products. The assumed weighting factor for the effective dose equivalent relative to whole-body exposure is 0.08

^c Department of Energy facilities, smelters, transportation, etc.

360 mrem, per year. Most of this exposure, ~80%, is natural background radiation, and about two-thirds of that is from radon. Radon results from the decay of uranium, a ubiquitous natural component of the earth's crust, and subsequently decays to plutonium. Both radon and plutonium are trans-uranic elements and thus undergo α -decay, with the emission of densely ionizing, high-LET α -rays (radiation weighting factor, $w_R = 20$). Radon is a gas and so is inhaled with the ambient air. If it decays to plutonium, a solid, while still within the lungs, the solid plutonium particle will not be exhaled but will be deposited on the surface of the pulmonary epithelium. When the plutonium subsequently undergoes α -decay in situ, a high dose equivalent (24 mSv = 2,400 mrem) is delivered to the lung and a large contribution to the effective dose equivalent (2.0 mSv = 200 mrem) results. Only ~20% of the background radiation (0.6 Sv, or 60 mrem, per year) is from man-made sources, and almost all of this is due to medical exposures; note that this 60 mrem-per-year effective dose equivalent represents an average among all members of the US population, including those who have and those who have not had an actual medical exposure. Other specific exposures, both medical and non-medical, are presented in Table 1.5. Diagnostic medical exposures range from 4 mrem for a chest X-ray at the low end to 830 mrem for a chest CT at the high end, with nuclear medicine exposures (e.g., that from a ^{99m}Tc bone scan) generally in the middle of this range. The miscellaneous non-medical exposures range from 6 mrem for a trans-Atlantic commercial airline flight to 400 mrem per year from natural background radiation in Denver, CO. The foregoing dose estimates provide some perspective on radiation exposures: effective dose equivalents of several hundred to a thousand millirem, comparable to those received by diagnostic nuclear medicine patients and personnel, appear not to be associated with any grossly demonstrable adverse health effects.

10CFR35 stipulates radiation protection standards for occupationally exposed individuals (such as nuclear medicine technologists and physicians) as well as for non-occupationally exposed individuals. These standards are based on the assumption – the no-threshold hypothesis – that any radiation dose above natural background may create some additional risk of damage – hereditary defects, potential life-span shortening, and, in particular, cancer. Thus, it is prudent to design a radiation safety program that maintains radiation doses to workers and the public not just below the regulatory limit but as low as reasonably achievable (ALARA). The annual maximum permissible doses (MPDs) for radiation workers are currently as follows: effective dose equivalent, 50 mSv = 5 rem; dose equivalent to any one tissue or organ except the eye, 500 mSv = 50 rem; and dose equivalent to eye, 150 mSv = 15 rem.

Table 1.5. Radiation doses in perspective: effective dose equivalents for selected medical and non-medical exposures

	Effective dose equivalent (mrem)
Medical exposures	
Chest X-ray	4
Sentinel node procedure (breast)	32
Mammogram	40
Brain CT	180
^{99m}Tc bone scan	360
Intravenous urography	460
Barium enema	500
Abdominal CT	720
Chest CT	830
Non-medical exposures	
Trans-Atlantic airline flight ^a	6
Annual dose to nuclear medicine technologists – US average	180
Annual natural background radiation – US average	360
Annual natural background radiation – Denver, CO ^a	400

^a The additional dose in Denver, CO, and the dose in a trans-Atlantic airline flight are due to increased cosmic radiations at these higher altitudes

The respective MPDs to non-occupationally exposed individuals are one-tenth of the corresponding MPD for occupationally exposed individuals, including an effective-dose-equivalent limit of 5 mSv, or 0.5 rem, per year. For the general public at large, as opposed to specific non-occupationally exposed individuals (such as a secretary in a nuclear medicine facility), the MPD is an effective dose equivalent of 1 mSv, or 0.1 rem. Finally, for a declared pregnant worker (i.e., an occupationally exposed individual who has informed her employer of her pregnancy), the MPD over the total duration of her pregnancy is the same as that of a non-occupationally exposed individual, 5 mSv = 0.5 rem.

1.5.4 Personnel Dosimetry

For occupationally exposed individuals, personnel monitors provide estimates of external exposure. Personnel monitors typically achieve an accuracy of $\pm 30\%$ and a precision of $\pm 10\%$ over an exposure range of 10 mR (the lowest detectable exposure) to 2,000 R with constancy (i.e., constant signal per unit exposure) over a wide X- and γ -ray energy range. Until recently, commercially supplied and processed “film badges” consisted of plastic holders containing a small piece of X-ray film in a light-tight seal. The optical density, or opacity (“blackening”), of film is directly related to its exposure. Thermoluminescent dosimeters (TLDs) have now largely replaced film in personnel monitors. TLDs

are composed of crystalline solids (most commonly, lithium fluoride, LiF), which can be formed into small disks or rods. When TLDs absorb radiation energy and are subsequently heated to sufficiently high temperatures, they emit visible light in an amount directly related to the radiation energy absorbed. "TLD readers" consist of a light-tight oven in which the TLD is heated, a PMT to detect and measure the light emitted by the TLD, and associated electronics. Prior to use (i.e., exposure to radiation), each lot of film or TLDs must be calibrated to yield a lot-specific "calibration factor" (i.e., optical density or light emitted, respectively, per unit radiation dose). Unlike film, TLDs are re-usable and, after being read out but before being re-used, must be super-heated (or annealed) to stimulate the emission of spurious (non-radiogenic) light. Among the desirable characteristics of TLDs are sensitivity (to exposures as low as ~ 10 mR), linear, energy-independent response, and insensitivity to heat, light, and humidity as well as re-usability. Incidental heating after radiation exposure but prior to readout may dissipate the light signal and thus yield a spuriously low signal.

Personnel dosimeters typically have a metallicity filtered area (to provide an estimate of the "deep" dose) and an unfiltered area (to estimate the shallow, or "skin," dose). Both film and TLDs are "integrating" detectors and thus yield the total dose up to the time the film is developed or the TLD is read. Personnel dosimeters are generally changed monthly. Most radiation workers wear a single dosimeter, typically on the trunk of the body. Certain cohorts of workers such as radiopharmacists may wear additional dosimeters (e.g., ring and eye glass dosimeters).

1.5.5

Receipt, Transport, Storage, and Inventory of Radioactive Materials

Radioactive packages should be examined and opened on disposable pads wearing disposable gloves. Packages should be inspected immediately upon receipt for any sign of damage such as breakage, moisture, or discoloration of the outer packing. As soon as possible after receipt, packages should be monitored for external radiation levels using a survey monitor and possible surface contamination determined by wipe testing (see below). If the measured exposure rate is not consistent with the package label or if it appears that the package is damaged, the RSO or designee shall be contacted immediately. Once a package is opened, the inner container should be inspected for any breakage or leakage and wipe tested for contamination. The inner container label and the packing slip should be cross-checked to verify the vendor, the identity and physical and chemical forms of the radionuclide, the activity present and date and time of calibration. Any deviations should be re-

ported to the shipper and resolved. The packing material and empty package should also be monitored for radioactive contamination using a survey meter before disposal. If radioactively contaminated, these materials should be treated as radioactive waste. If free of contamination, the radiation/radioactivity labels should be removed or obliterated before appropriate disposal as non-radioactive waste.

Radioactive packages cannot be transported in the same manner as non-radioactive packages and must be shipped by UD DOT-authorized "dangerous-goods" carriers. A completed "dangerous-goods" manifest, listing the names and addresses of the shipper and the consignee, the radionuclide and its activity and chemical and physical forms, a 24-h emergency contact telephone number, and the transport index (see below), must accompany the shipment. In addition, US DOT-authorized "radioactive shipment" labels must be completed and affixed to at least two surfaces of the radioactive package (Fig. 1.21).

All vials or other vessels that contain radioactive materials should be labeled appropriately with "Caution Radioactive Material" warnings and provide the identity of the radionuclide, physical and chemical forms of the radionuclide, activity, date and time of calibration. Such items should be stored in shielded (lead) containers and the containers stored in shielded cabinets or drawers or behind lead shielding. For certain radiopharmaceuticals that must be stored at low temperatures, a refrigerator may be lined with lead or a refrigerator may be located in an appropriately shielded area. Radioactive materials should be stored in secure, controlled areas, such as a radiopharmacy, posted with "Caution Radioactive Material" warning signs. If personnel inside these areas could receive a dose rate of 0.05 mSv/h (5 mrem/h) or more, the door should be posted with a "Caution Radiation Area" sign. Items such as food, beverages, and medications shall not be stored in the same area as radioactive materials. A running inventory of radioactive materials must be maintained. This inventory should include: the identity of the radionuclide, physical and chemical forms of the radionuclide, activity, date and time of calibration and of receipt activities dispensed and the dates and times of dispensing and the patient or other purpose for which it was dispensed; the activity, date and time, and method of disposal.

1.5.6

Radiation Surveys

Radiation surveys should be performed using a survey meter (such as a Geiger counter) calibrated in absolute exposure rate or absorbed dose rate units (mR/h or mrad/h, respectively). Because of the limited penetration of β -rays and other particulate radiations, the abil-

ity of each type of survey meter to detect these radiations should be clearly understood. The use of beta shields or caps may allow for measurements in fields of mixed radiations. Survey meters should include a “battery check” function. Some models may include a low-activity “check source” to provide a check on operation of the instrument immediately prior to use. These devices shall be calibrated at least annually and records of the calibrations shall be maintained.

Removable radioactive contamination can be deposited on skin or enter the body and irradiate an individual internally. Therefore, assay of removable radioactive contamination on all potentially contaminated surfaces and on sealed radioactive sources must be performed at regular intervals and whenever contamination is suspected. Non-removable radioactive contamination, i.e., fixed contamination, contributes only to external exposure and its contribution is reflected in the radiation surveys. Assay of removable radioactive contamination is typically performed using a “wipe test.” In such a test, a representative area of approximately 100 cm² of a potentially contaminated surface is wiped with a dry piece of paper and the wipe is counted in a counting system. The resulting gross count rates are converted to net count rates by subtracting a background, or blank, count rate and the net count rates converted to activity using the counting system’s measured calibration factors.

In controlled, or restricted, areas, surveys should be performed daily and wipe tests weekly. In other (uncontrolled or unrestricted) areas, surveys should be performed weekly and wipe tests monthly.

1.5.7

Waste Disposal

Nuclear medicine generates low-level radioactive waste, mostly in the form of dry waste (such as empty vials, syringes, intravenous tubing, disposable gloves, absorbent pads, paper toweling, gauze, contaminated disposable eating utensils, and partially decayed sources). Regulations concerning disposal of radioactive or radioactively contaminated waste are stringent: no waste which is detectably radioactive (i.e., yields a count rate significantly greater than the background count rate when assayed with a high-sensitivity survey meter) may be disposed of as non-radioactive waste. Depending on a facility’s volume of radioactive waste and its capacity for waste storage, disposal may be accomplished by one or more of the following methods: return to vendor, decay-in-storage, transfer to a radioactive waste facility (commercial disposal), and, for liquid waste, dilution and dispersal.

Radioactively contaminated dry waste that will decay to background levels within a reasonably short period of time (i.e., up to several months) should be

stored for decay. Such storage locations should be in a low-occupancy, secure and posted area of the facility and adequately shielded as required. Prior to disposal or recycling of decayed radioactive waste, such materials should be monitored with a suitable survey meter to verify that radioactivity is undetectable, and all “radioactive-material” labeling should be removed or obliterated prior to disposal or recycling. Radioactive or radioactively contaminated waste should be segregated by physical half-life to facilitate final disposal. Many hospitals have installed high-sensitivity counting systems to monitor *all* waste exiting the facility and, if necessary, divert at that point radioactively contaminated waste for decay-in-storage. Low-level, non-infectious liquid radioactive waste as well as excreta (including excreta collected in urine bags and bedpans) from nuclear medicine patients generally may be disposed of by dilution or dispersal, that is, disposal down a waste drain or toilet. The facility’s radiation safety officer must assure that liquid radioactive waste discharged into the sewer does not exceed regulatory limits. Radioactivity and radioactively contaminated waste too long-lived to be practically held for decay-in-storage [such as carbon-14 ($T_{1/2} = 5,730$ years) and tritium ($T_{1/2} = 12.3$ years)] must be disposed of commercially (for eventual encasement, transport to, and long-term burial at one of only several low-level radioactive waste sites nationwide). Commercial disposal is extremely expensive, but, fortunately, is rarely required in nuclear medicine.

1.5.8

Radionuclide Therapy and the “New” Release Criteria

Historically, the NRC and Agreement States required radionuclide therapy patients to remain hospitalized until the retained activity in the patient was less than 1,110 MBq (30 mCi) or the dose rate at 1 m from the patient was less than 0.05 mSv/h (5 mrem/h). In 1997, however, the NRC amended its regulations concerning radionuclide therapy patients through the issuance of new rules that appeared in the Federal Register on January 29. The new NRC regulations, revised 10CFR 35.75 effective May 1997, allow for the release from medical confinement of patients if the expected total effective dose equivalent (TEDE) to individuals exposed to the patient is not likely to exceed 5 mSv (500 mrem). Guidance on determining when patients may be released based on the new criteria, when written instructions on post-release radiation precautions must be provided, and when records related to the release of the patient must be maintained are provided in NRC Regulatory Guide 8.39. A licensee may release from his or her control any patient administered (diagnostic or therapeutic) radiopharmaceuticals or therapeutically implanted with sealed radioactive sources if the TEDE to any indi-

vidual from exposure to the patient after release is not likely to exceed 5 mSv (500 mrem). Compliance with this dose limit may be demonstrated using either: (a) a default table in Regulatory Guide 8.39 for activity (e.g., <33 mCi of iodine-131 retained by the patient) or dose rate (e.g., <7 mrem/h at 1 m from an iodine-131-containing patient) or (b) patient-specific kinetic data using effective half-times or residence times and dose rate measurements and a patient-specific projected dose calculation. The use of method (b) will generally result in patients being released with substantially higher activities – up to several hundred mCi – than would method (a). Importantly, in basing release on patient-specific information [method (b)], the NRC regulations allow for representative kinetic data such as effective half-times or residence times for a particular population of patients (e.g., hyperthyroid patients) to be applied to an individual patient in that population, thus obviating the need in certain cases for measurement of kinetic data on an individual patient basis. The revised NRC regulations require that the licensee provide written instructions to the released patient regarding radiation precautions. Post-release radiation safety instructions to the patient should address maintenance of distance from other persons, separate sleeping arrangements, minimization of time in public places including public transportation facilities such as buses, trains, and planes, and measures to reduce environmental contamination. In the case of nursing mothers, recommendations on discontinuation of breast-feeding should be included as well. Information on the duration of post-release radiation precautions must also be provided. The revised NRC regulations impose, under some circumstances, certain record-keeping requirements. If patient release is based on method (a), records are not required. However, if release is based on method (b), a record of the basis for release including patient-specific factors and dose-calculation equations must be prepared and maintained for 3 years from the date of release.

1.5.9

Record-Keeping

Written and/or computerized records, maintained for periods established by regulatory agencies and/or the facility, are required. The required records and other documentation include the: radioactive materials receipt, inventory, distribution, and disposal, including radiopharmaceutical prescriptions; radiation survey data, including measurements of ambient radiation levels and surface radioactive contamination, and annotated facility diagrams indicating the sites of such measurements; monitoring records for all occupationally exposed personnel, including any bioassay data; written policies and procedures for the clinical and the

radiation-safety program; description of the radiation-safety training program; the Radiation Safety Committee membership and minutes; and reports of any unusual, radiologically significant occurrences.

1.5.10

“Sensitive” Patient Populations

The administration of radioactive materials, even in diagnostic amounts, to certain “sensitive” populations – pregnant women, nursing mothers, and prospective parents – remains a matter of concern in nuclear medicine.

Pregnant Women. Increasingly accurate anatomic models of the fetus and pregnant woman have been developed, including models of the pregnant female at the beginning of pregnancy (representing the embryo as a small unit density sphere located at the uterus) and at the end of the first and third trimesters. Radiopharmaceutical kinetic data in utero and therefore fetal dose estimates are quite limited, however. Published fetal absorbed dose estimates are generally of the order of or less than 0.1 cGy (0.1 rad) per 37 MBq (1 mCi) administered to the mother. A particularly worrisome issue, however, is radioiodine administration to pregnant women. The fetal thyroid begins concentrating iodine at the 12th to 15th week of gestation. At 16–24 weeks, ¹³¹I-iodide delivers a very large absorbed dose of 1,500–6,000 cGy/37 MBq (rad/mCi) to the fetal thyroid and an absorbed dose of 3–5 cGy/37 MBq (rad/mCi) to the fetal total body, depending on maternal thyroid uptake. For a hyperthyroid therapy administration of 185 MBq (5 mCi), 7,500–30,000 cGy (rad) would therefore be delivered to the fetal thyroid and 15–25 rad to the fetal total body. Not surprisingly, with radiogenic destruction of the fetal thyroid and thyroid hormone deficiency in utero, fetal hypothyroidism and congenital cretinism have been shown to result following radioiodine therapy of hyperthyroidism or thyroid cancer in pregnant women. It is therefore critical to avoid radioiodine administration to the pregnant patient, even in diagnostic amounts.

Nursing Mothers. Diagnostic radiopharmaceuticals administered to lactating women can achieve rather high concentrations in breast milk and potentially deliver significant radiation doses to nursing infants. For example, the cumulative breast milk activity ranged from 0.03% to 27% of ¹³¹I-iodide administered to six women for thyroid uptake studies. Using a variety of dosimetric criteria [e.g., an effective dose equivalent to the nursing infant of 0.1 cSv (0.1 rem)], a number of authors have recommended different interruption periods prior to resuming breast-feeding following administration of radiopharmaceuticals. While there is no absolute consensus, the following are representative

of the published recommendations: 24 h following any administration of ^{99m}Tc or ^{18}F , 2–4 weeks following administration of ^{67}Ga -gallium citrate, and permanently for the current nursing infant following any administration of ^{131}I -iodide.

Prospective Parents. No evidence of significant germ cell damage (indicated by an increased risk of birth defects among subsequently conceived offspring) has been observed among A-bomb survivors (average gonadal absorbed dose: > 30 cGy) and exposed human cohorts and no such damage is expected, therefore, among diagnostic nuclear medicine patients. Nonetheless, demonstrable gonadal damage, specifically, *transiently* impaired fertility, may occasionally occur among thyroid cancer patients treated with much larger amounts (> 100 mCi) of ^{131}I followed by full recovery of fertility. While it is difficult to rationally formulate guidelines on the basis of the limited human data available, it is perhaps prudent that patients forego starting a family for at least several months following such high-dose radioiodine therapy.

1.5.11

Concluding Remarks

Based on the preponderance of negative (“no-effect”) results from radiation epidemiology studies in the dose range of the order of 1 rem, in diagnostic nuclear medicine the activities used and the associated radiation doses are generally so low that there is no practical possibility of any short- or long-term demonstrable harm to patients, staff, and other individuals. However, because of the large relative increase in the risk of child-

hood cancer following even low-level exposures in utero, radiation (including nuclear medicine) procedures in pregnant women must be based on an informed and *documented* decision regarding medical necessity. This, and *not* the possibility of inducing fetal death or congenital abnormalities, is why females of child-bearing age are routinely queried about the possibility of being pregnant prior to undergoing a radiological or nuclear medicine procedure.

Further Reading

- Bendriem B, Townsend DW (eds) (1998) The theory and practice of 3D PET. Kluwer Academic, Dordrecht
- Cherry SR, Sorenson JA, Phelps ME (2003) Physics in nuclear medicine, 3rd edn. Saunders, Philadelphia, PA, pp 325–359
- Zanzonico PB (1995) Technical requirements for SPECT: Equipment and quality control. In: Kramer EL, Sanger JJ (eds) Clinical applications in SPECT. Raven Press, New York, pp 7–41
- Zanzonico P (2000) Internal radionuclide radiation dosimetry: A review of basic concepts and recent developments. *J Nucl Med* 41:297–308
- Zanzonico P (2002) The intraoperative probe: design, operation, and safety. In: Cody HS III (ed) Sentinel node biopsy. Martin Dunitz, London
- Zanzonico P (2004) Positron emission tomography: A review of basic principles, scanner design and performance, and current systems. *Semin Nucl Med* 34:87–111
- Zanzonico P, Heller S (2000) The intraoperative gamma probe: Basic principles and choices available. *Semin Nucl Med* 30:33–48
- Zanzonico P, Siegel J, St Germain J (2000) A generalized algorithm for determining the time of release and the duration of post-release radiation precautions following radionuclide therapy. *Health Phys* 6:648–659